The Meteoritical Society

Meteoritics & Planetary Science 56, Nr 8, 1531–1555 (2021)
doi: 10.1111/maps.13712

Evaluating urban micrometeorites as a research resource—A large population collected from a single rooftop

M. D. SUTTLE[1], T. HASSE[2], and L. HECHT[2,3]*

[1]Planetary Materials Group, Department of Earth Sciences, Natural History Museum, Cromwell Road, London SW7 5BD, UK
[2]Museum für Naturkunde, Leibniz-Institut für Evolutions- und Biodiversitätsforschung, Invalidenstr. 43, Berlin 10115, Germany
[3]Institut für Geologische Wissenschaften, Freie Universität Berlin, Malteserstraße 74-100, Berlin 12249, Germany
*Corresponding author. E-mail: lutz.hecht@mfn.berlin

(Received 28 October 2020; revision accepted 12 May 2021)

Abstract–We report the recovery and characterization of a new urban micrometeorite collection derived from the rooftop of an industrial building in Germany. We identified 315 micrometeorites (diameter: 55–515 μm, size peak: ~150 μm, size distribution slope exponent: −2.62). They are predominantly S-type cosmic spherules (97.2%) but also two G-type spherules (0.6%), an unmelted coarse-grained single-mineral micrometeorite, and eight scoriaceous particles (2.5%) or particles transitional between scoriaceous micrometeorites and porphyritic spherules. Their analysis details how the magnetite rim on partially melted micrometeorites is progressively diluted as the melt fraction increases during heating. At least 10 micrometeorites contain platinum group nuggets (PGNs). They have chondritic compositions but are depleted in volatile Pd. However, a single nugget preserves chondritic Pd concentrations. We suggest that an Fe-Ni-S bead originally containing the PGN escaped its host cavity and wet the particle exterior, creating an Fe-rich melt that protected the nugget from evaporation. This melt layer oxidized forming magnetite—indicating that wetting events can affect the texture and composition of micrometeorites. Utilizing the well-constrained surface area (8400 m^2) and rooftop age (21 yr), we attempted the first global mass flux estimate based on urban micrometeorite data. This produced anomalously low values (13.4 t yr^{-1}), even when correcting for losses due to sample processing (<89.7 t yr^{-1}). Our value is approximately two orders of magnitude lower than previous estimates, indicating that >99% of particles are missing, having been lost via drainage and cleaning. Rooftop collection sites have limited potential for mass flux calculations unless problems of loss can be resolved. However, urban micrometeorite collections have other advantages, notably exceptionally well-preserved particles with extremely young terrestrial ages and the ability to extract many micrometeorites from accessible sites. Urban micrometeorites should be considered complementary to Antarctic and deep-sea collections with potential for citizen science and educational exploitation.

INTRODUCTION

Micrometeorites are grains of cosmic dust with sizes between 50 and 3000 μm (Taylor et al. 2000; Genge et al. 2008; Folco and Cordier 2015; Suttle and Folco 2020). They are derived from asteroids (e.g., Brownlee et al. 1997; Van Ginneken et al. 2012) and comets (Duprat et al. 2007; Noguchi et al. 2015). Once released from their parent body, cosmic dust spirals into the inner solar system and is either captured by terrestrial planets or consumed by the Sun (Nesvorný et al. 2003, 2006). Numerical models suggest that a large proportion of the impinging micrometeorite flux reaching the Earth completely evaporate during atmospheric entry (potentially up to 90%, Love and Brownlee 1991; Taylor et al. 1998; Carrillo-Sánchez et al. 2015). Among the particles which do survive, a further ~90% suffer complete melting (Love and Brownlee 1991). Molten

droplets form subspherical shapes, pulled in by surface tension—they are termed cosmic spherules and represent the most abundant form of cosmic dust found at the Earth's surface (Taylor et al. 2007; Genge et al. 2008). They are further subclassified based on chemical composition into silicate-dominated (S-types [representing ~97% of all cosmic spherules, Taylor et al. 2000]), iron-dominated (I-types), and an intermediate class composed of silicate glass with embedded magnetite (G-types; Genge et al. 2008).

Micrometeorites were first recognized among terrestrial sediments in the late 1800s. Nordenskiöld (1874) described minute magnetic black particles containing Fe, Ni, Co, and P. These particles had been recovered from sea-ice north of Spitsbergen, from Greenland ice, and from snow in Stockholm. Nordenskiöld suggested they were cosmic dust that had been removed from the atmosphere by precipitation. Later, Murray and Renard (1891) identified cosmic spherules among the deep-sea sediments recovered from the ocean floor during the HMS Challenger expedition (1872–1876). Their report includes impressive hand-drawn figures showing both the exterior and interior of various particles, several of which have textures consistent with cosmic spherules (Murray and Renard 1891, see pages 327–336 and plate XXIII).

Studies throughout the 1940–1960s attempted to recover micrometeorites from various environments, including urban settings (Nininger 1941; Buddhue 1950; Handy and Davidson 1953; Schmidt 1965). Nininger (1941) reported large numbers of magnetic spherules collected in urban areas and suggested these were cosmic spherules. However, their abundances were found to decrease with distance from urban centers, leading Handy and Davidson (1953) to conclude that the particles were fly-ash—non-combustible material derived from the burning of fossil fuels. Instead, Handy and Davidson (1953) argued that the presence of Ni should be considered essential diagnostic criteria (and combined with the observation of small size, black/metallic appearance, subspherical shapes, and attraction to a magnet) before particles can be confidently identified as micrometeorites. Consequently, from the 1950s onward, the notion that micrometeorites could be recovered from urban environments was considered an urban myth, unsupported by scientific research.

Throughout the late 20th century and early 21st century, renewed interest in micrometeorite research led to the recovery of cosmic spherules from deep ocean sediments (Blanchard et al. 1980; Murrell et al. 1980; Brownlee et al. 1984, 1997; Rudraswami et al. 2011; Prasad et al. 2013). Deep sea derived micrometeorites were the first cosmic spherules to be studied systematically using electron beam techniques. Brownlee et al. (1997) demonstrated that most spherules have CM-like compositions and are affected by depletions in siderophile and volatile elements. Furthermore, owing to their long residence in corrosive seawater, many of these particles were also affected by etching, dissolution, and alteration. As a result, increasingly research effort was directed toward the recovery of micrometeorites from Antarctica, and initially from blue ice. Sites like Cap Prud'homme (Maurette et al. 1991), the South Pole Water Well (SPWW, Taylor et al. 1998, 2000), and the Dome Fuji Water Well (Yada et al. 2004) provided an abundance of micrometeorites (<700 μm). This included unmelted representatives that had previously not been found. Later, micrometeorites were recovered from Antarctic snow (notably the CONCORDIA collection, Duprat et al. 2001, 2007), leading to the discovery of a new class of unmelted micrometeorites (termed ultracarbonaceous Antarctic micrometeorites [UCAMMs]) with affinities to comets (Dobrică et al. 2009, 2012). They are rare, highly friable particles with high carbon contents, abundant organic matter, extreme deuterium excesses, and isotopic $\delta^{15}N$ enrichments (Duprat et al. 2010; Noguchi et al. 2015). Micrometeorites have also been recovered from Antarctic subaerial sediment traps, both moraines (Genge et al. 2018) and weathering pits (deep and narrow cracks in the tops of the Transantarctic Mountains [Suttle and Folco 2020]). Interestingly, the Transantarctic Mountain micrometeorite collections were, until recently, the only source of giant micrometeorites (with particle sizes up to 3000 μm, Rochette et al. 2008; Suavet et al. 2009; Suttle et al. 2019; Goderis et al. 2020). Their presence is likely due to the long accumulation times (>800,000 yr) of these traps.

Although Antarctic micrometeorite collections have several obvious benefits, they also suffer drawbacks. Antarctica is a difficult region to access meaning that sampling missions are often prohibitively expensive. Furthermore, subaerial collection sites have long and often poorly constrained accumulation ages (Suttle and Folco 2020) meaning that most particles within these traps are heavily affected by terrestrial weathering (Van Ginneken et al. 2016). Such long terrestrial residence times also deleteriously affect some analytical techniques and thus limit the research potential of micrometeorite collections (e.g., Antarctic micrometeorites are suboptimal for implanted noble gas studies [e.g., Stuart et al. 1999; Osawa et al. 2003]). Conversely, micrometeorites that must be extracted from ice or snow often require melting the water-ice and thus contact with liquid water. The isotopic composition of Antarctic water is light (low $\delta^{18}O$ values around $-55‰$, Lodders and Fegley 1998) and even short duration

exposure can result in compromised isotopic compositions in some particles (Suttle et al. 2021), although most particles appear to escape extraction without significant alteration (e.g., Engrand et al. 1999; Gounelle et al. 2005; Yada et al. 2005).

The discovery that micrometeorites can be successfully recovered from urban environments is therefore an important development in the field of micrometeorite research. Recently, particles recovered by Jon Larsen as part of Project Stardust from rooftops in Oslo (and later elsewhere) were confirmed as cosmic spherules (Genge et al. 2017a; Larsen 2017, 2019). Among 500 particles collected, Genge et al. (2017a) analyzed 48 in detail using electron microprobe analysis (EMPA) and backscatter electron imaging (BSE) under scanning electron microscope (SEM). Further analysis of the remaining particles confirmed that all the potential micrometeorites collected by Larsen were extraterrestrial. This discovery gained significant media attention, motivating numerous researchers and amateur scientists to attempt their own collection efforts (e.g., Peterson 2020 [Micro-meteorites project: https://micro-meteorites.com], Hasse 2020 [Urban micrometeorites: www.micrometeorites.org]) and inspiring several new citizen science projects (e.g., Blake et al. 2018; Micrometeorites—The Cosmic Treasure of Berlin Roofs [2019]—a joint citizen science initiative, led by the Museum für Naturkunde Berlin and the Freie Universität Berlin which aimed to collect micrometeorites from rooftops across the city; Esposito et al. 2020).

Here, we characterize a new collection of 315 urban micrometeorites all recovered from a single rooftop above a furniture store in Meppen, Germany. This case study explains in detail the recovery techniques required for successful micrometeorite collection from urban areas—thereby providing a pilot study that may be copied by future researchers, amateur micrometeorite hunters, large-scale citizen science projects, and/or school groups. Furthermore, by considering only micrometeorites recovered from a single rooftop, we explore the utility of urban collections for constraining the mass flux of extraterrestrial material falling to Earth at the present day. Both the age and area of this rooftop are known, essential criteria for an accurate flux calculation. Finally, we show petrographic data from several partially melted micrometeorites, a first among urban micrometeorite collections.

METHODS

Location, Processing Technique, and Recovery

The flat rooftop examined on July 9–10, 2019 belongs to a furniture store on the outskirts of Meppen (52°40′14.8″N, 7°18′4.6″E), a city in Germany with a population of approximately 35,000. The owner granted permission to enter for the investigation. The roof area of this study was approximately 8400 m^2, of which approximately 7500 m^2 were able to be sampled. It is a plastic roof with a series of linear drainage profiles and internal drains. The height of the roof edge finish varies between approximately 15 and 50 cm. The age of the roof is 21 years. Despite the usual work to keep the drains clear, well over 100 kg (estimated) of sediment has accumulated on the roof. There are two sedimentation regimes which were sampled separately (as outlined in Table 1):

1. Precipitation-bound deposits in the low-lying gutters and around the drains.
2. Aeolian (wind-blown) deposits on the sheltered edges and in the corners of the roof.

At the time of sampling, the rooftop sediment was dry, which is a prerequisite for the method used: All the sediment was first swept up into numerous small piles. Each pile was hand-sieved (<800 μm) in portions for approximately 10 s each and the remaining fine material was collected. It was then spread in portions forming 2–3 mm thick flat layers and magnetic particles were extracted from the sample using a strong neodymium round magnet (Ø 48 mm, 143 g). For this purpose, the magnet was guided over the entire sample at a distance of approximately 1 cm. The sample was then remixed, spread out again, and the procedure repeated (1–2 times). The magnet was covered with a plastic film so that the adhering particles could be detached frequently from the magnet and collected. The resulting magnetic extraction was taken to the laboratory for further treatment. In addition, we collected and investigated a random sample (approximately 3%) of the nonmagnetic aeolian deposit and a random sample (again, approximately 3%) of the coarse-grained material (>800 μm) discarded during hand sieving.

Sediments were then separated in the laboratory into five different size fractions (425–800 μm, 250–425 μm, 150–250 μm, 100–150 μm, <100 μm). Each fraction was cleaned separately using hot water with the addition of washing-up liquid. Low-density particles were decanted. This was achieved by stirring the sample vigorously and leaving the container for a short time (1–6 s depending on the size fraction treated, waiting longest for the smallest size fraction), thereby allowing the high-density particles to settle to the base of the container while the lower density particles remained in suspension and were subsequently poured away. The container was then refilled with water and this step repeated several times until only high-density particles

Table 1. Sample masses and number of micrometeorites (MMs) separated by different sediment regimes and separation steps.

	Mass (<800 μm) after sieving (g)	Mass of magnetic fraction (g)	Mass after washing (g)	No. of MMs found in washed fraction	No. of MMs recovered from decanted fraction	No. of MMs found in a 3% sample of discarded nonmagnetic fraction
Air-bound sediment	~15,500	33.5	16.3	224	16	13
Water-bound sediment	~3000	10.1	2.5	39	2	
Mixed/unclear source	~2500	7.0	2.7	20	1	

that sunk rapidly to the base of the container were left. This high-density aliquot was then dried. Meanwhile the wet (low-density) decanted material was collected with a 100 μm sieve, dried, and a final magnetic separation effort undertaken on this aliquot. Both aliquots (the washed high-density fraction and the magnetic extract from decanted low-density fraction) were then searched under binocular microscope for potential micrometeorites.

The above processing steps on the roof and in the laboratory ensure that low-density particles, weakly magnetic and nonmagnetic particles, as well as particles with sizes less than approximately 50 μm are removed. These grains are overwhelmingly anthropogenic or natural terrestrial material. Similar density separation techniques have previously been employed in the processing of Antarctic sediments (e.g., Suttle and Folco 2020). Processing is necessary to make micrometeorite extraction feasible and is achieved by the passive enrichment of cosmic dust among the remaining terrestrial sediment. However, we acknowledge that this treatment regime will have the effect of inadvertently removing some micrometeorites (generally small—approximately <100 μm in size—and nonmagnetic particles).

Identifying Micrometeorites

This subsection outlines the optical, textural, and chemical criteria used in this study to positively identify micrometeorites.

Most micrometeorites recovered in this study are cosmic spherules. These are extraterrestrial dust grains that have completely melted and recrystallized during atmospheric entry. As a result, much of their mineralogy and textures are dominated by the late-stage quench cooling process. Cosmic spherules are characterized by small sizes (typically 50–500 μm) and subspherical morphologies. They typically have dendritic or porphyritic crystallites suspended in a glassy mesostasis (Khisina et al. 2016; Larsen 2017, 2019) and may also contain vesicles (Genge 2017), sulfide beads (Taylor et al. 2011), and/or Fe-Ni metal beads (Genge et al. 2017a) exposed at their exterior.

The three chemical subdivisions of cosmic spherule (S-type, I-type, and G-type) have distinct compositions, and this affects their characteristic appearance and the diagnostics of identification. The silicate-dominated S-types often appear black; gray; or more rarely brown, green, or whitish and have vitreous luster when fresh (unweathered). They often show different characteristic patterns on their surface (e.g., barred olivines, large olivine crystals) and/or shapes (e.g., turtleback, egg-shaped). They have chondritic bulk compositions but with depletions in volatile elements (Brownlee et al. 1997; Genge et al. 2008; Cordier et al. 2011). By contrast, the I-type spherules (which were not found in this study but included in this description for completeness) are composed almost entirely of Fe-Ni metal. During atmospheric entry, they progressively oxidize to form Fe-oxides. Consequently, the I-type spherules often have a bright gray-to-silver appearance and strong metallic luster. Their major mineral phases are Ni-rich metal and Ni-bearing wüstite and magnetite (Genge et al. 2017b). Due to their resemblance with industrial spherules, I-type micrometeorites are particularly difficult to identify under the light microscope. The G-type spherules are relatively rare (~1% of particles, Taylor et al. 2000) and have compositions intermediate between the S-type and I-type. They contain magnetite dendrites suspended in an Mg-Fe-rich silicate glass (Genge et al. 2008).

In addition to cosmic spherules, we also recovered a small number of scoriaceous micrometeorites (ScMMs). These partially melted particles often have highly vesicular textures and high porosities (10–50 vol%, Kohout et al. 2014; Dionnet et al. 2020). They have irregular to subspherical shapes with smooth rounded or subrounded external surfaces and gray metallic appearance (owing to the presence of a magnetite rim). Scoriaceous micrometeorites (and unmelted particles) can be identified by the presence of a dense covering or envelope of magnetite crystals that surround the micrometeorite's outer surface. This is termed a magnetite rim (Genge et al. 2008).

Chemical Analysis and Optical Imaging

All sediment samples treated in the laboratory were optically searched for micrometeorites with a binocular stereomicroscope (MBS-10 CSSR, max. magnification 56×) equipped with a ring-shaped LED light. Particle color, shape, and surface texture (including characteristics such as metal/sulfide beads and cavities) were used for selecting potential micrometeorites (a total of 468 candidate particles were picked under optical microscope, of these 315 proved to be extraterrestrial). Light images were taken with a combination of a Canon EOS 80D camera, a Zeiss Axioscope microscope, self-constructed light equipment, and photo stacking and graphic manipulation software (for a complete set of images, see supporting information in Hasse et al. 2021).

Uncoated particle exteriors were then analyzed under SEM. We used a JEOL/EO JSM-6610LV series SEM operating in low vacuum mode and with an accelerating voltage of 15 kV and an unmeasured beam current. The stage was held at a 14 mm working distance and particles were imaged with BSE imaging and their chemical compositions analyzed using standardless energy dispersive X-ray spectrometry (EDS) collected on their topographically complex surfaces. Here, we employed a Bruker XFlash 5010 spectrometer and processed the resulting data with the Esprit software (v2.1). For these initial analyses, we rastered the electron beam over a large and representative region of each particle's exposed surface area to obtain a rough estimate of their chemical composition. In addition, when analyzing specific phases exposed at the particle surface (e.g., the PGNs), point analyses using the spot mode were employed. Analyses on the metal "crusts" used either spot or area analyses, altered to suit the specific size/shape of the phase under investigation.

Several studies have collected geochemical data from cosmic spherule–hosted PGNs (Brownlee et al. 1984; Bonté et al. 1987; Rudraswami et al. 2011, 2014). These analyses remain challenging, owing to the small size of PGNs (leading to problems of beam overlap with the surrounding matrix), their position on cosmic spherule exteriors (generating topographically complex surfaces which contradict ZAF quantification assumptions), and the presence of multiple highly refractory elements with overlapping Kα peaks. Despite these limitations, most studies have published data which are scientifically consistent with astrophysical processes (i.e., siderophile element abundances in PGNs occur at chondritic abundances) and are thus likely close to the true PGN's composition. Previous studies often employed EDS (as opposed to EMPA) owing to the benefits of higher spatial resolution (smaller beam spots and more accurate targeting). Likewise, in this study, we also used EDS and analyzed exposed PGNs on spherule exteriors. Although conditions are suboptimal, the resulting data (see Table 3) carry similar uncertainties to previously reported studies, allowing a direct comparison. To further reduce uncertainty, we normalized element abundances against Ir concentrations (following conventional data handling as in Tagle and Berlin 2008), producing elemental ratios that carry lower uncertainties than absolute concentrations.

A subset of the micrometeorite population (50 particles) were then set in epoxy resin, sectioned, and polished to expose their interiors (of which two were plucked from the resin during polishing and lost). The sectioned particles were subsequently carbon-coated and reanalyzed under SEM at high vacuum. We used an accelerating voltage of 15 kV, an unmeasured beam current, and a fixed working distance (13 mm). These improved analysis conditions (avoiding topographic artifacts induced by rough samples) allowed the collection of higher accuracy chemical data (EDX analyses) (Fig. 1). In addition, polishing allowed the internal textures of these micrometeorites to be investigated. The accuracy of EDS analyses (on the sectioned micrometeorite interiors) was checked by collecting compositional data on a San Carlos olivine mineral standard during the same analysis session (Fig. 1).

RESULTS

Size Distribution

In total, 315 micrometeorites (see supplementary data in Hasse et al. 2021) were recovered in this study from the rooftop. They range in size between 55 and 515 μm. The entire micrometeorite population can be displayed as a rank–size distribution (Fig. 2), which plots the cumulative number of micrometeorites greater than a given diameter. This plot demonstrates that the micrometeorite population analyzed here has a deficit in both large (>340 μm) and small (<100 μm) particles. Over the size range (100–340 μm), two trend lines were fitted to the data—a power law (with a slope of −2.62, $R^2 = 0.93$) and an exponential function (with an exponent of −0.014, $R^2 = 0.98$).

Plotting the size data as a size–frequency distribution (histogram function, Fig. 3) demonstrates that the collection approximately follows a skewed normal distribution with a peak in micrometeorite abundance located at 160 μm and with additional smaller peaks at larger particle diameters (220 and 340 μm).

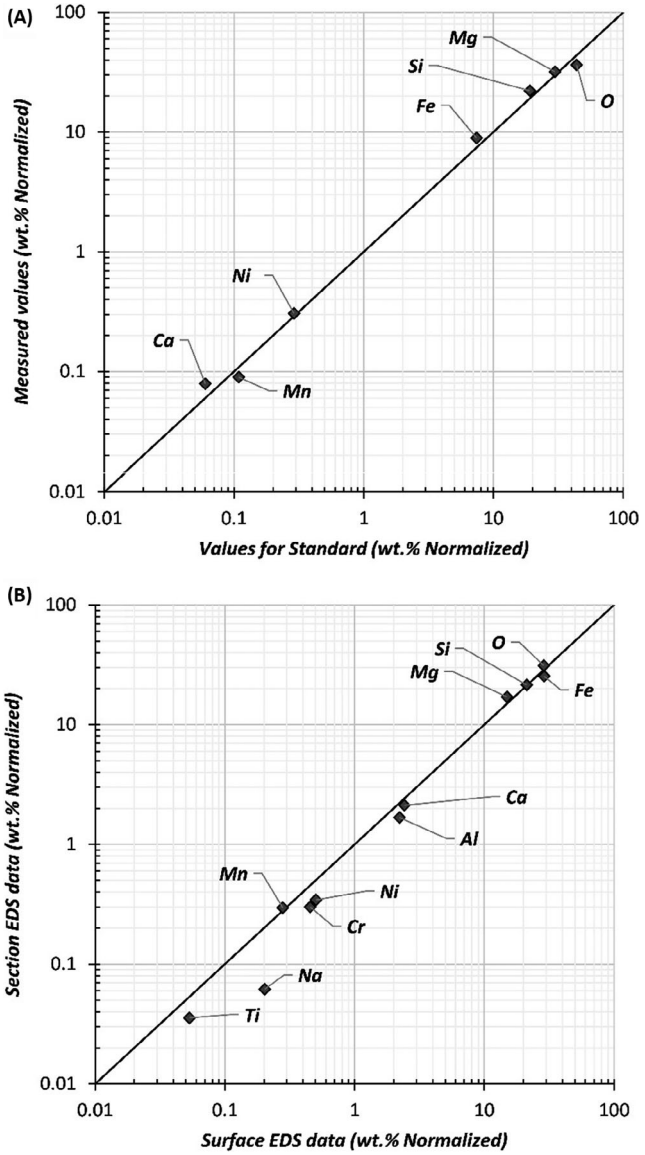

Fig. 1. Comparing the accuracy of EDX analyses collected using the JEOL/EO JSM-6610 series, SEM employed in this study. A) Averaged repeat analyses on our internal San Carlos olivine mineral standard (Jarosewich et al. 1980; Ca abundance data taken from De Hoog et al. 2010) are compared against our EDX analyses of the same standard. This demonstrates that spot analyses performed on flat, polished surfaces are accurate for all elements whose abundance occurs at concentrations >0.5 wt%. Elements <0.5 wt% can be detected, but their values carry higher error. B) In this study, we collect chemical data from both micrometeorite external surfaces and their flat polished sectioned interiors. The average surface and sectioned compositions are compared here. This plot indicates that surface analyses (which are known to be more inaccurate) tend to overestimate most element abundances. Surface EDS analyses should therefore be used cautiously with knowledge of their limitations.

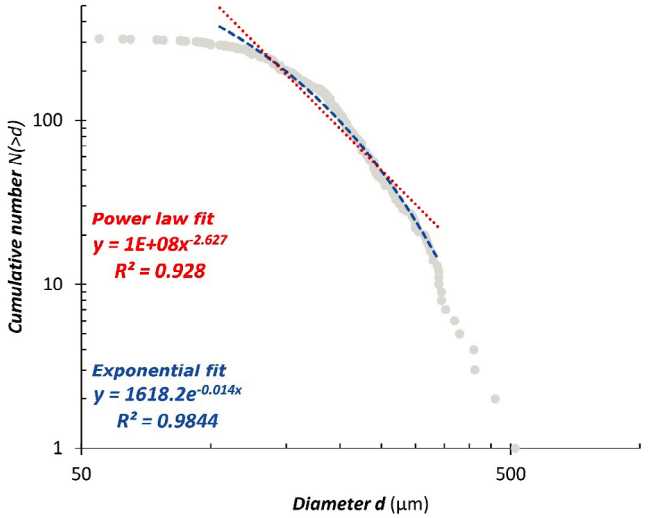

Fig. 2. A rank–size distribution plot for the 315 micrometeorites analyzed in this study and recovered from a single rooftop. The main population (279 particles) is fitted against both a power law (shown in red) and an exponential function (shown in blue). Fit statistics and equations showing the slope and exponent functions are given. (Color figure can be viewed at wileyonlinelibrary.com.)

Textural Classification

Cosmic spherules are subdivided on the basis of quench textures into different groups (Figs. 4 and 5). Owing to the excellent preservation state among the Meppen particles, cosmic spherules could be provisionally assigned textural subtype based solely on analysis of their external surface textures. This is not usually possible for subaerial Antarctic micrometeorites whose surfaces are affected by terrestrial weathering and/or have mineral encrustations (e.g., Van Ginneken et al. 2017). Although we are relatively confident in our provisional classification, the 48 sectioned particles allowed us to test this initial surface-based classification. Among these 48, six received a revised classification. In most instances that was a relatively minor alteration (e.g., identification of a relict phenocryst hidden inside the particle demanded reclassification as a porphyritic [PO] spherule, or realization that the crystal grain size within the micrometeorite interior differed slightly from the exterior, leading to a change from cryptocrystalline [CC] to barred olivine [BO]). Micrometeorite population statistics are given below.

In total 315 micrometeorites were recovered in this study, of these 306 (97.1%) were found to be cosmic spherules. Almost all of these cosmic spherules (n = 304) belong to the silicate-dominated chemical class of cosmic spherules (96.8%), termed the S-types. They can be

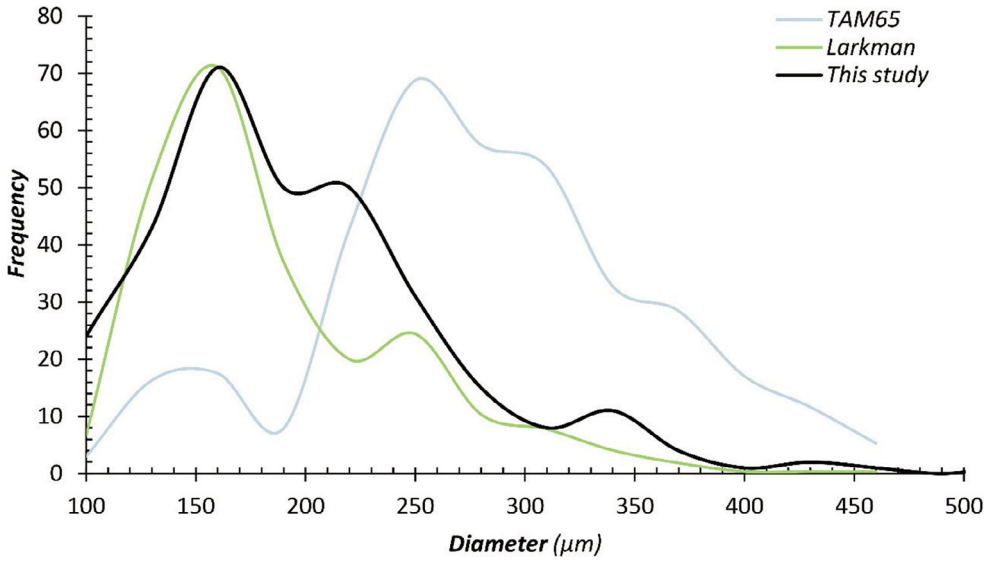

Fig. 3. Size–frequency distribution plot for the micrometeorites analyzed in this study and comparison against the size distribution data from the TAM65 micrometeorite collection (Suttle and Folco 2020) and the Larkman Nunatak micrometeorite collection (Genge et al. 2018). Micrometeorite abundance follows a skewed normal distribution with a main peak at 160 μm (this is in close agreement with the presence of abundance peaks in other Antarctic micrometeorite collections). Additional shoulder peaks are seen at 220 and 340 μm. The presence of multiple peaks, as opposed to a simple normal distribution, indicates that the micrometeorite flux is composed of multiple sources each with distinct size distributions; these different sources sum to produce the multi-peaked profile observed. The presence of a main peak at 160 μm found in both urban and Antarctic micrometeorite collections increases confidence that this is a true feature of the micrometeorite flux and not an artifact of how the micrometeorite collections are processed. (Color figure can be viewed at wileyonlinelibrary.com.)

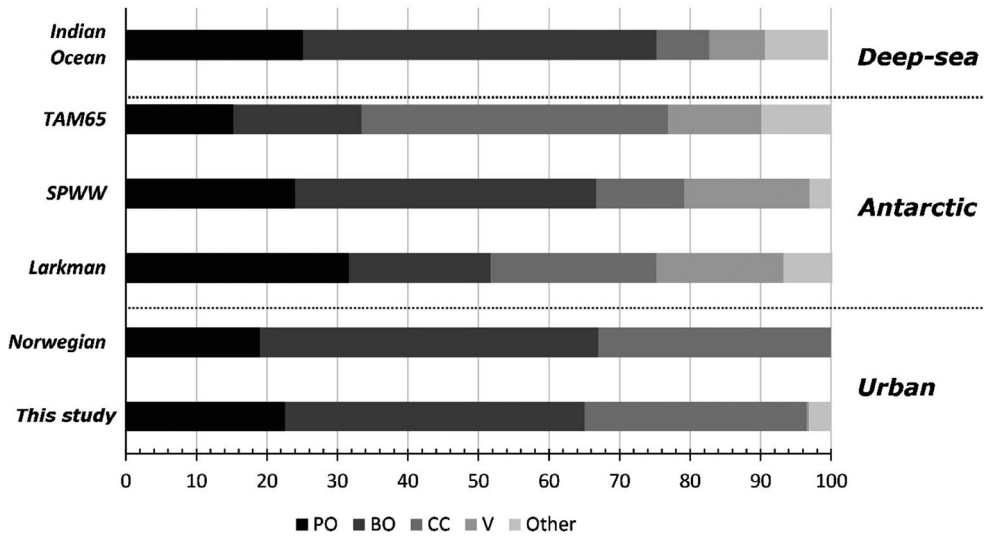

Fig. 4. Cosmic spherule population statistics. This plot compares the relative abundance of different quench textures in the present urban micrometeorite population against other established micrometeorite collections, including the Indian Ocean collection (Prasad et al. 2013), Antarctic collections (Taylor et al. 1998, 2000; Genge et al. 2018; Suttle and Folco 2020), and the 500 particles in the first urban micrometeorite collection (Genge et al. 2017a).

further subdivided based on their quench textures. Among the cosmic spherule population, 23.2% of particles (n = 71) are PO (Figs. 5C–F), 38.6% (n = 118) are BO (Figs. 5G and 5H), 37.1% (n = 114) are CC, and 0.3% (a single particle [THMM418]) is glassy (V-type [for vitreous, Figs. 5O and 5P]). As in Suttle and Folco

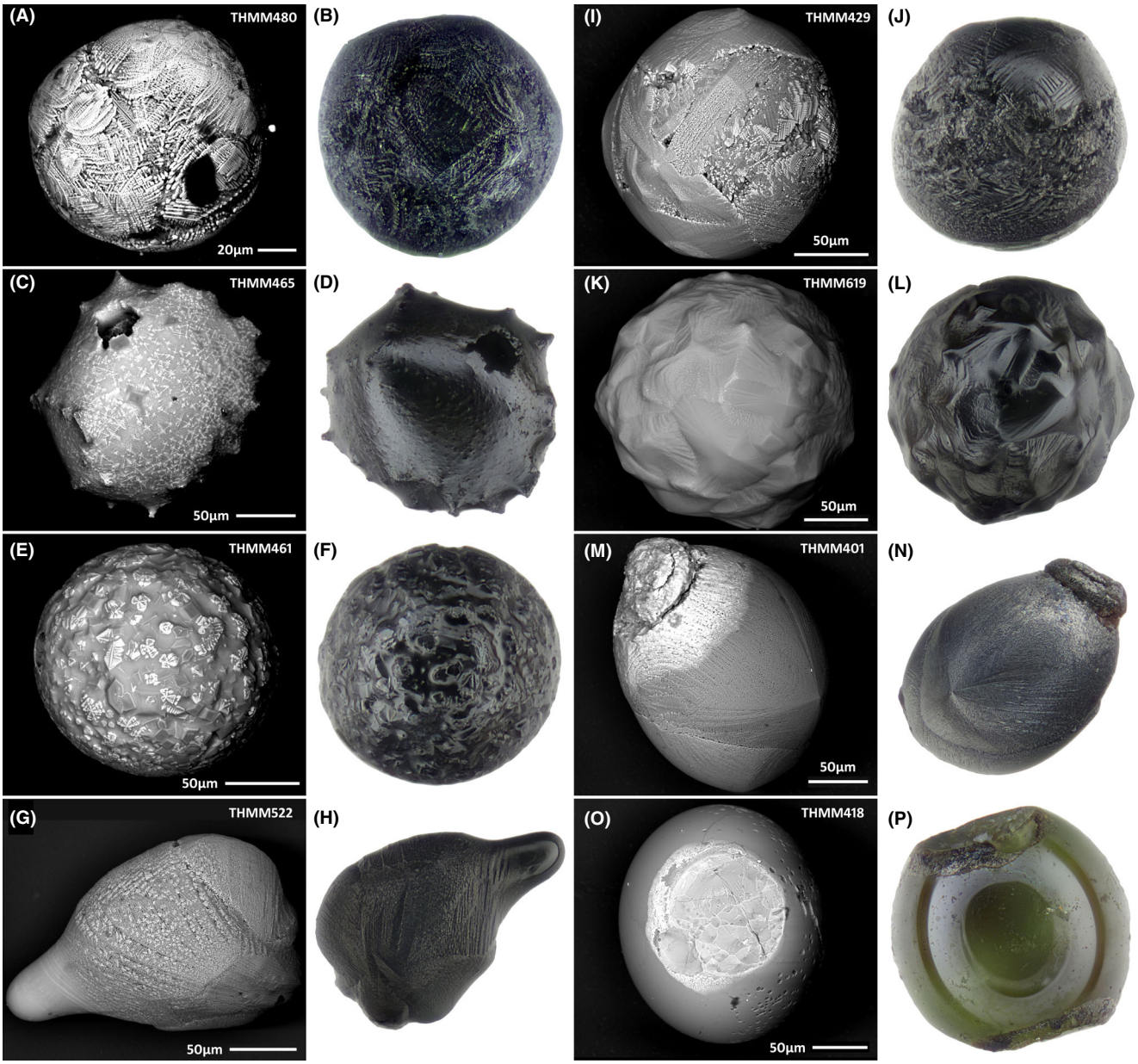

Fig. 5. Example images of different cosmic spherule textural subtypes, presented as SEM-BSE and optical pairs (with minor sample reorientation between images)—A and B: the G-type spherule, C and D: a PO spherule with several microtails, E and F: a PO spherule, G and H: a BO with a large tail, I–N: cryptocrystalline spherules representing the three different subgroups: microcrystalline (I and J), turtleback (K and L), and normal (M and N—which also shows an Fe-Ni-S bead wetting event), O and P: a vitreous (glass) spherule with two large metal beads on opposite sides of the spherule. These were lost during the particle cleaning process (in the ultrasound instrument). (Color figure can be viewed at wileyonlinelibrary.com.)

(2020), we further separated the CC class into three distinct textural groups: microcrystalline (MC [24.8% (n = 76), Figs. 5I and 5J]), which have localized regions with a barred texture as well as regions with randomly orientated olivine and magnetite crystals; CC-normal (7.5%, n = 23 [Figs. 5M and 5N])—these have no evidence of barred texture and instead are composed entirely of randomly orientated olivine and magnetite. The final subclass are the CC-turtleback particles (CC-Turt. [4.8%, n = 15 Figs. 5K and 5L]). They have multiple well-defined crystal domains that form a stitched texture and often contain few or no magnetite crystals (as described in Brownlee et al. [1983]; Taylor and Brownlee [1991]; Genge et al. [2008] and others).

In addition to the S-type cosmic spherules, we identified two G-type spherules (0.6% of the population

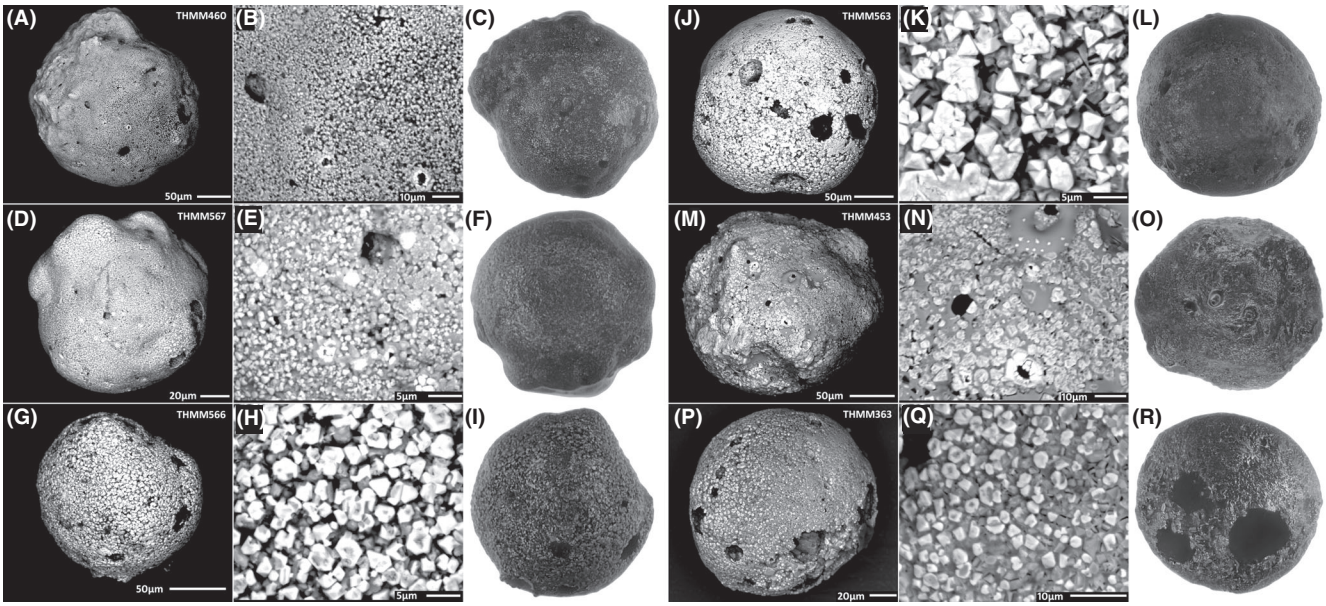

Fig. 6. A–R) Backscatter and optical images of scoriaceous micrometeorites recovered in this study. They exist on the spectrum between the partially melted (scoriaceous [ScMM]) micrometeorites and PO cosmic spherules. Several particles have magnetite rims, which are diagnostic characteristics of unmelted and partially melted micrometeorites. However, they also have rounded surfaces and subspherical shapes—properties associated with cosmic spherules and occurring where high melt fractions pull the particle into a spherical shape to minimize surface tension.

[THMM455 and THMM480, Figs. 5A and 5B]) and eight particles that are partially melted and span the morphological spectrum between scoriaceous micrometeorites (ScMMs) and porphyritic spherules. They are here grouped for simplicity as ScMMs (Fig. 6). Finally, we identified a single particle (THMM465) that initially appeared to be an S-type cosmic spherule, but following sectioning was recognized as an unmelted coarse-grained micrometeorite (CgMM) dominated by a single mineral surrounded by a thin layer of melt (termed an igneous rim) and lacking a magnetite rim. It remains possible that other particles in this collection could also be unmelted single mineral micrometeorites misidentified as cosmic spherules; however, single mineral micrometeorites are relatively rare (Genge et al. 2008; fig. 3 in Taylor et al. 2012), and therefore, this type of misclassification will be a rare occurrence.

Bulk Chemical Compositions

In addition to textural characteristics, chemical analyses were used as further evidence to confirm extraterrestrial origin. All 315 particles received at least one chemical analysis (collected on their external surface). In addition, the 48 sectioned particles (see supplementary data in Hasse et al. 2021) also received at least one wide beam analysis collected on their polished interiors, used to infer their approximate bulk composition (Table 2; Fig. 7). All particles have chondritic compositions with the vast majority of element abundances varying within one order of magnitude of CI chondrite values. In general, refractory Al and Ca show elevated abundances relative to our Ivuna standard (up to 2x and 4x), while moderately refractory elements (Si, Mg, and Fe) have flat profiles. Nickel consistently shows depletions below CI values, typically in the range 0.1–0.9x and Cr varies between ~1.5x and 0.2x CI values. Depletions in both Ni and S are features common to most micrometeorites and are routinely attributed to loss by co-evaporation alongside sulfur, ejection of high-density Ni-rich beads (Brownlee et al. 1997), or by leaching during terrestrial weathering and contact with liquid water (Kurat et al. 1994). Volatile elements (e.g., S, K, and Na) have low concentrations, typically below CI values and, in most cases, below the detection limits of our analytical setup.

Comparing Surface and Sectioned EDS Data

Because we collected wide beam EDS analyses on both particle exteriors and sectioned interiors for 48 particles, differences in the estimated bulk composition between these two approaches can be evaluated (Fig. 1).

Table 2. Average bulk compositions for different micrometeorite subtypes and bulk compositions for selected spherules. Data displayed as wt% normalized.

Particle ID	Classification	*N*=?	Na	Mg	Al	Si	P	S	Ca	Ti	Cr	Mn	Fe	Ni	O	Total
–	ScMM (Avg.)	12 (3)	0.1	14.6	2.6	17.4	b.d.l.	0.1	1.6	0.1	0.3	0.2	33.5	0.8	28.5	100.0
–	ScMM (1σ)		0.2	3.0	1.9	2.2	–	0.2	0.4	0.2	0.1	0.0	4.0	0.4	0.9	–
–	PO (Avg.)	24 (14)	0.1	18.9	1.3	22.2	b.d.l.	b.d.l.	1.6	b.d.l.	0.4	0.3	23.4	0.3	31.4	100.0
–	PO (1σ)		0.2	4.1	0.4	3.7	–	0.1	0.7	0.1	0.2	0.2	8.4	0.5	2.4	–
–	BO (Avg.)	10 (10)	b.d.l.	15.8	1.8	20.3	0.0	0.1	2.6	b.d.l.	0.4	0.2	28.2	0.3	30.3	100.0
–	BO (1σ)		–	2.2	0.3	2.2	0.1	0.2	1.1	–	0.1	0.1	6.2	0.5	1.6	–
–	CC (Avg.)	18 (17)	b.d.l.	17.2	1.6	22.5	b.d.l.	b.d.l.	2.4	b.d.l.	0.2	0.3	23.7	0.1	32.1	100.0
–	CC (1σ)		–	2.5	0.4	3.1	–	–	1.2	–	0.2	0.2	6.3	0.3	1.8	–
THMM418	V	1 (1)	b.d.l.	17.3	1.5	24.1	b.d.l.	0.2	0.6	b.d.l.	0.6	0.4	23.1	b.d.l.	32.2	100.0
THMM453	ScMM	4 (1)	b.d.l.	16.2	1.7	18.9	0.1	0.1	2.1	b.d.l.	0.4	0.3	30.4	0.3	29.5	100.0
THMM460	ScMM	4 (1)	0.3	17.3	1.7	18.5	0.1	0.4	1.1	b.d.l.	0.5	0.2	30.4	0.7	29.0	100.0
THMM567	ScMM	4 (1)	0.1	14.6	1.5	18.1	b.d.l.	b.d.l.	1.6	b.d.l.	0.3	0.2	34.4	1.2	27.9	100.0
THMM465	CgMM (single min.)	1 (1)	b.d.l.	22.7	0.3	21.9	b.d.l.	b.d.l.	0.4	b.d.l.	b.d.l.	0.4	21.8	b.d.l.	32.5	100.0
THMM455	G-type	1 (1)	b.d.l.	7.1	6.0	18.6	b.d.l.	b.d.l.	6.1	0.2	0.3	b.d.l.	29.3	3.1	29.3	100.0
THMM480	G-type	1 (1)	0.0	10.4	5.5	14.1	b.d.l.	b.d.l.	1.7	0.4	0.2	0.2	38.8	1.0	27.6	100.0

b.d.l. = below the detection limit. In the "*N*=?" column, the number outside the parentheses denotes the total number of independent analyses averaged to produce the compositional data, while the number in parentheses denotes the number of separate particles included in the calculation.

Surface-derived EDS analyses collected on topographically complex materials are generally considered to be low quality. This is because the uncontrolled geometry affects X-ray generation and propagation, leading to shadowing effects and resulting in systematic errors in quantification (Newbury and Ritchie 2013). This is particularly problematic with SEM systems that rely on a single detector mounted on one side of the chamber, rather than annular SSD geometries (Salge et al. 2014). Despite these drawbacks, analysis of cosmic spherule exteriors by EDS is becoming a more common practice. It is therefore important to evaluate how reliable surface EDS data can be. In the present study, we found that, on average, surface EDS analyses routinely produce mild underestimates for Mg, Fe, and O abundances by approximately 2.0–3.5 wt%, while overestimating other elements such as Ca (on average by ~0.3 wt% or ~35%) and Al (on average by ~0.5 wt% or ~60%). As a result, surface EDS analyses when combined with BSE images showing characteristic quench textures can be treated as a useful tool in separating micrometeorites from industrial and other terrestrial spherules. However, quantification should be treated with appropriate caution and only used for preliminary work, or where sectioning is not practical (e.g., when analyzing phases that are preferentially located on the outside of micrometeorites such as metal/sulfide coats or platinum group nuggets [PGNs]).

Siderophile and Chalcophile Beads

A common feature found exposed at the surfaces of cosmic spherules are beads composed either of Fe-Ni-metal and/or Fe-Ni-sulfides. In this collection, 54 particles or 17.1% of the collection have at least one bead exposed at their surface. These abundances are similar to the ~20% value given in Suttle and Folco (2020). Most of the exposed beads are S-bearing (~60%) while 45 contain detectable Ni—among these 18 contain more Ni than Fe.

In addition to Fe-Ni(-S) beads, some particles contain micron-sized refractory-rich PGNs. They are significantly less common (2.9% of the population [Fig. 8]). We identified PGNs in nine S-types and one G-type (THMM480). Their sizes and chemical compositions are shown in Table 3 and plotted in Figs. 9 and 10. They range in size from 0.3 to 1.6 μm and contain sufficiently high Ru, Rh, Pd, Os, Ir, and Pt to be detectable by EDS. All nuggets have broadly chondritic elemental abundances and compositions consistent with literature data on previously reported PGNs in cosmic spherules (Fig. 9).

Fine-Grained Partially Melted (Scoriaceous) Micrometeorites

We identified eight particles (THMM361, THMM363, THMM453, THMM454, THMM460, THMM563, THMM566, and THMM567 [a subset of

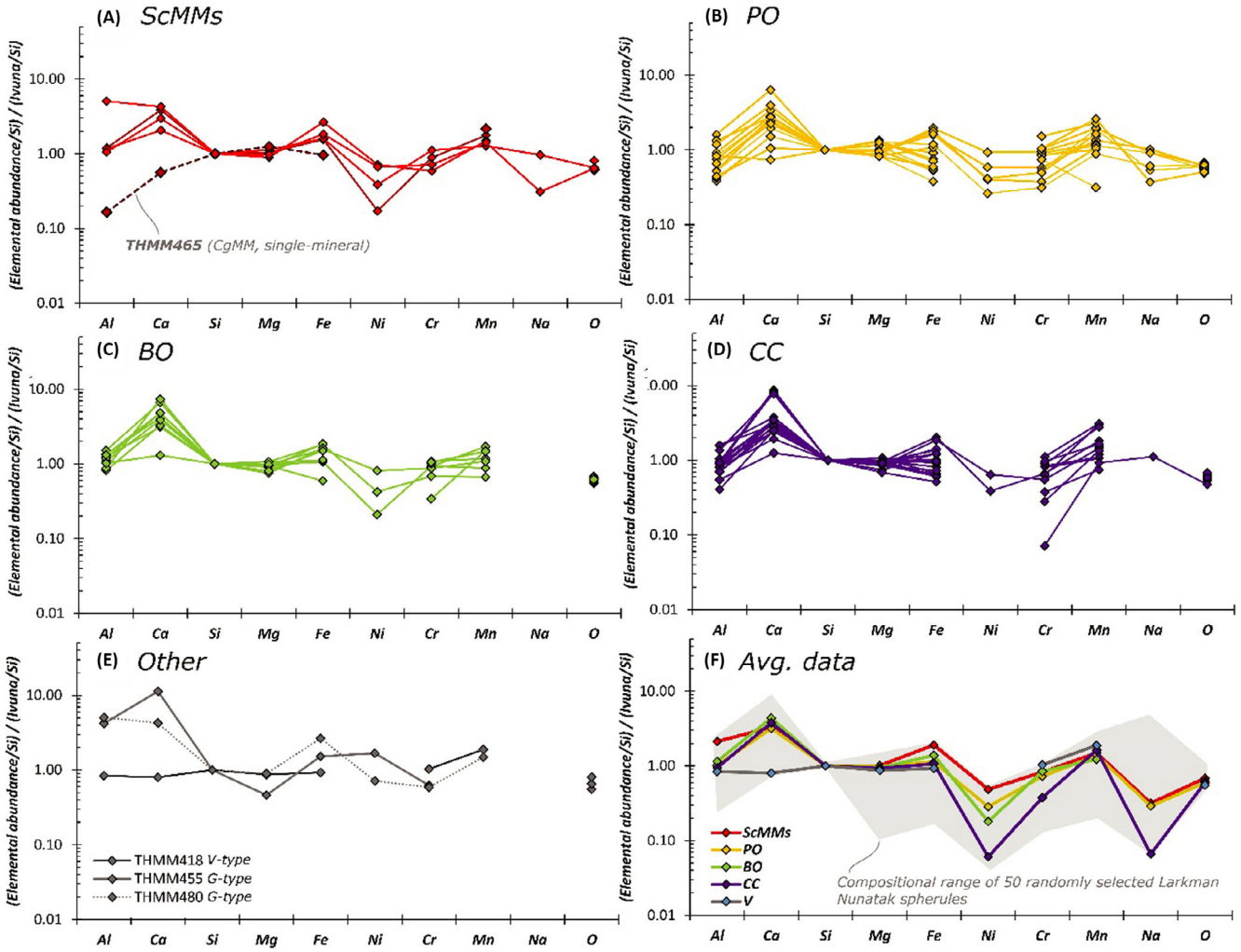

Fig. 7. Geochemical data (obtained as standardless EDS analyses collected on micrometeorite flat sectioned interiors) for 48 randomly selected urban rooftop micrometeorites. Data are normalized to both Si and CI chondrite compositions and elements are ordered by volatility. Panels represent different textural subclasses of micrometeorite. A) Scoriaceous micrometeorites, (B) PO spherules, (C) BO spherules, (D) CC spherules, (E) the single V-type and the two G-type micrometeorites, and (F) averaged compositions by textural subtype, compared against the compositional range of 50 Larkman Nunatak S-type cosmic spherules (marked by the gray shaded region). This plot demonstrates that the urban micrometeorites have chondritic bulk compositions (generally within one order of magnitude of the CI Ivuna composition). Deviations from chondritic compositions can be understood as a product of atmospheric entry and random subsampling of their parent body mineralogy. Mildly elevated abundances of refractory elements and corresponding depletions in volatile elements are typical of flash heated micrometeorites and reflect the preferential evaporation of volatile elements. Depletions in Ni (and S) are also common and associated with metal bead ejection, and co-evaporation during sulfur loss (Taylor et al. 2011). Note where an element nondetection occurred (i.e., abundance below detection limits), these points have been omitted from the plot. (Color figure can be viewed at wileyonlinelibrary.com.)

which are shown in Fig. 5]) which have ScMM-like characteristics, including irregular and/or subspherical shapes with rounded edges and at least a partial magnetite rim. Their external surfaces are frequently punctuated by (ruptured) vesicles, indicating volatile gas release during entry and high internal porosities in the quench-cooled particles. The outer magnetite rim may be composed of closely space euhedral magnetite crystals with rhombohedral and equant shapes (as in THMM563 [Figs. 5G–I]) or as smaller anhedral grains (as in THMM453 [Figs. 5M–O]). Discontinuous rims exposing silicate glass and neo-formed olivine grains or regions with a sparse covering of magnetite grains are also common on some particles, notably those with more spherical shapes (as in THMM363 [Figs. 5P–R]).

Among the particles that were sectioned (THMM453, THMM460, and THMM567), their interiors (Fig. 11) reveal textures consistent with

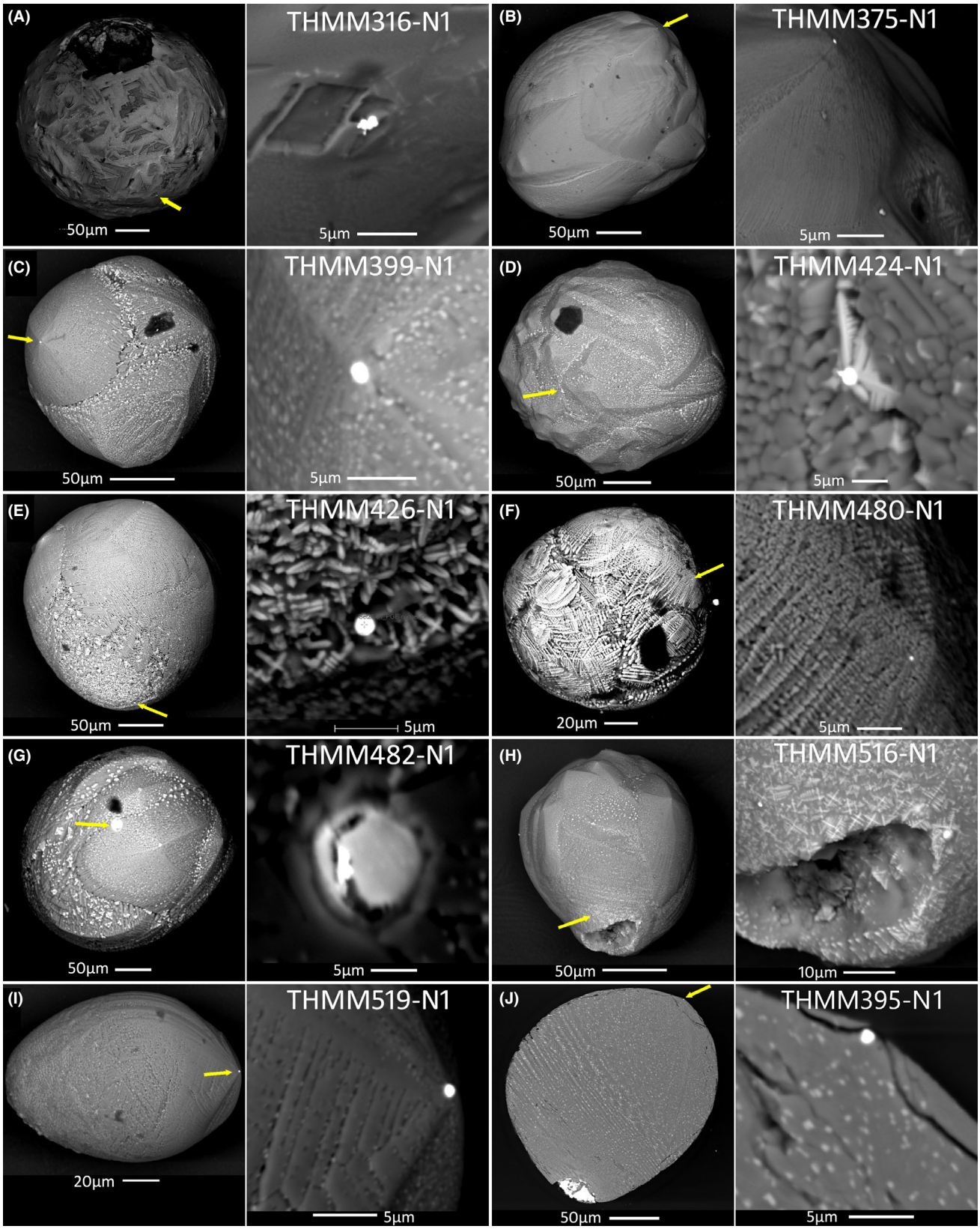

Fig. 8. A–J) Backscatter images of near-surface micron-sized PGNs, detected and analyzed by EDS measurements within 10 cosmic spherules (for each particle, an overview and high magnification image is shown). (Color figure can be viewed at wile yonlinelibrary.com.)

Table 3. Compositions of PGNs (the positions of each nugget on their host spherule are shown in Fig. 6). Compositions were determined by single point EDS measurement and are shown as normalized wt%, quoted to one decimal place. Approximate bead diameters are also given.

PGE nugget	Ø (μm)	Fe	Ni	Ru	Rh	Pd	Os	Ir	Pt	Total
THMM316-N1	1.3[1]	18.0	1.5	22.7	5.9	0.1	9.2	17.7	24.8	100.0
THMM375-N1	1.0	16.8	0.6	19.5	1.6	b.d.l.	13.9	22.1	25.6	100.0
THMM395-N1	*1.1*	*5.1*	*1.0*	*26.6*	*5.4*	*0.4*	*14.3*	*21.4*	*25.8*	*100.0*
THMM399-N1	1.3	68.8	2.7	6.9	0.9	3.4	3.2	6.4	7.8	100.0
THMM424-N1	0.8	26.7	b.d.l.	19.3	4.7	2.9	6.5	12.4	27.4	100.0
THMM426-N1	1.6	68.4	23.8	3.1	0.2	*b.d.l.*	b.d.l.	b.d.l.	4.5[2]	100.0
THMM480-N1	0.3	42.1	1.6	17.2	3.2	0.6	7.3	8.7	19.4	100.0
THMM482-N1[3]	1.0[1]	14.2	45.7	3.0	b.d.l.	0.5	b.d.l.	b.d.l.	36.7	100.0
THMM516-N1	0.6	11.8	75.6	3.2	0.6	2.2	1.4	1.4	3.7	100.0
THMM519-N1	0.9	6.1	1.6	23.3	5.4	7.6	10.4	15.3	30.3	100.0

b.d.l. = below the detection limit. Analysis THMM395 (shown in italics) is the only analysis performed on a sectioned flat surface, while the other nine analyses were conducted on topographically complex particle exteriors.
[1]Ellipsoid shape (potentially two merged nuggets).
[2]Values uncertain due to marginal position of PGN.
[3]Held within a larger Ni(Fe) metal bead.

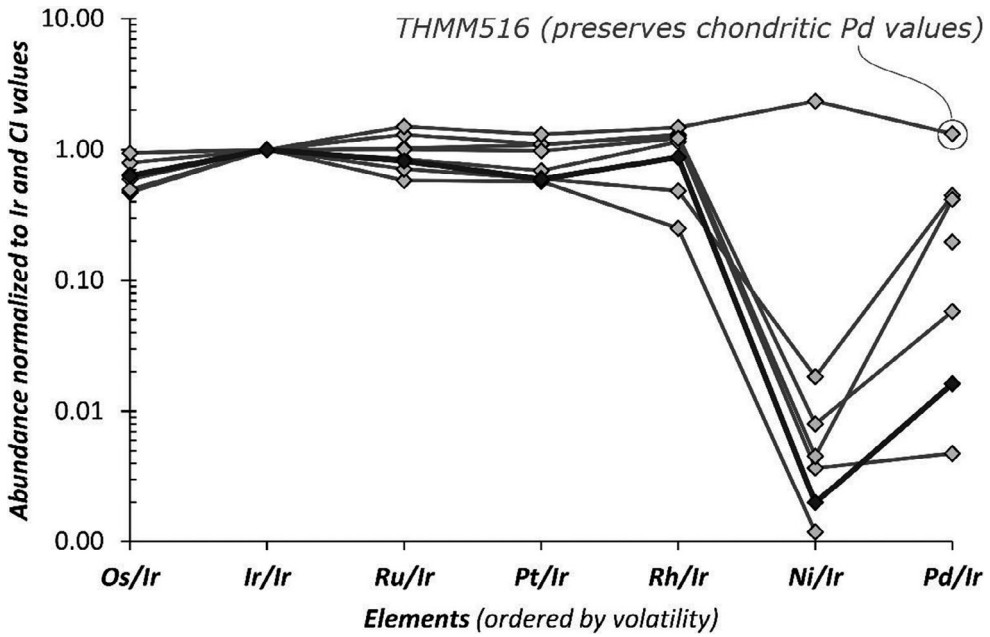

Fig. 9. Spider diagram of PGN compositions from seven S-type spherules and one G-type spherule. Data are normalized to CI chondrite compositions (obtained from Tagle and Berlin 2008). All nuggets have chondritic compositions with notable depletions in the more volatile elements (Ni and Pd). A single PGN (hosted within THMM516) appears to have avoided volatile depletion and thus preserves chondritic values for Ni and Pd. The dark gray line represents that analysis collected on the PGN in THMM395 (a sectioned EDS analysis, all others are surface EDS analyses).

scoriaceous micrometeorites. Particle THMM453 (Fig. 11A) contains several relict olivine grains with irregular shapes. They are enveloped by Fe-rich rims. Such normal zonation (Mg-rich cores [appearing dark in BSE images] and Fe-rich rims [appearing brighter in BSE images]) with sharp compositional boundaries are characteristic of relict olivine grains in micrometeorites and reflect the growth of Fe-rich olivine (mesostasis) during atmospheric entry (Steele 1992; Beckerling and Bischoff 1995; Genge et al. 2008). The matrix in THMM453 is dense, with relatively few vesicles. Instead, it is dominated by neo-formed Fe-rich olivine, Ca-rich silicate glass, and small equant magnetite crystals. An increased density of magnetite grains at the

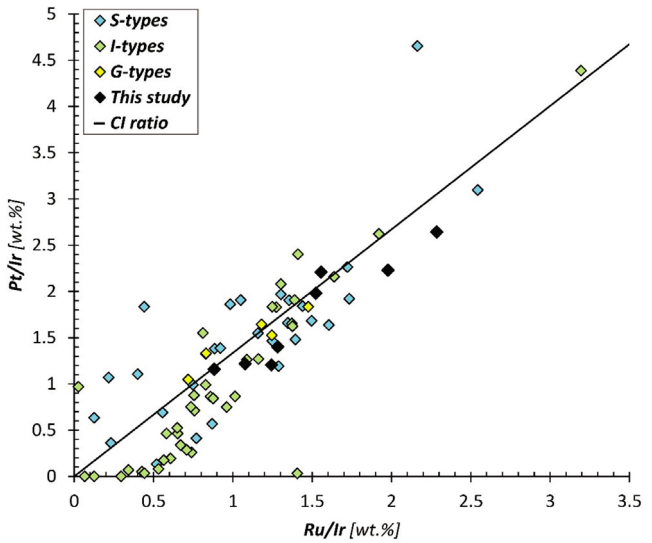

Fig. 10. Compositional data from PGNs exposed at the surfaces of six S-types and one G-type cosmic spherule derived from the Meppen micrometeorite collection (note that although we identified nine particles with PGNs, two lacked detectable Ir). The Meppen PGNs are compared against previously reported PGNs found in micrometeorites (S-, I-, and G-types). Data were taken from Brownlee et al. (1984), Bonté et al. (1987), and Rudraswami et al. (2011, 2014), while CI data were calculated from Tagle and Berlin (2008). All data are plotted as elemental ratios (calculated from their raw wt% data). We selected ratios since these are significantly more accurate than absolute abundance data. The PGN compositions of the Meppen particles were determined by standardless EDS on their topographically complex surfaces (raw data shown in Table 2). In contrast, literature data also used EDS but predominantly obtained from the polished flat surfaces of micrometeorite interiors. This plot demonstrates that the PGNs in micrometeorites (including those recovered from the Meppen rooftop) have chondritic elemental abundance for PGE elements. Furthermore, the similarity between PGN compositions in S-, I-, and G-type particles supports the conclusion that they all form in the same way from a chondritic source, concentrated by the oxidation of chondritic materials. (Color figure can be viewed at wileyonlinelibrary.com.)

particle perimeter and within the first ~20 μm margin inside the particle is clearly visible.

Particle THMM460 (Fig. 11B) retains three small relict olivine crystals as well as a cluster of Fe-sulfides that abut vesicles (identical to textures previously described by Taylor et al. [2011] for fine-grained scoriaceous micrometeorites). THMM460 is highly porous with numerous irregular-shaped vesicles; the remainder of the particle is composed of a nanocrystalline olivine groundmass. A thin (submicron) covering of magnetite grains at the particle margin can be seen in the sectioned image.

The sectioned interior of particle THMM567 (Fig. 11C) contains no relict grains. Like THMM460, this micrometeorite is dominated by a groundmass of nanocrystalline olivine grains with a uniform Fe-rich composition. Most of the internal volume of this particle is taken up by a single large, off-center vesicle with a rounded but irregular shape. It may therefore be described as a "hollow" particle, like those described in Genge (2017), they are inferred to form by high spin rates during atmospheric flight.

Tailed Cosmic Spherules

Seven micrometeorites in this population (2.2%) have well-defined tails (THMM411, THMM419, THMM420, THMM510, THMM522, THMM537, and THMM596 [Figs. 5G and 5H, and given in the supplementary data]), characterized by a long tapering extension of silicate melt, often found located at the opposite end of the particle from an exposed metal bead (e.g., THMM537). These extensions result in spherules whose shape deviates significantly from the ideal sphere. In addition to pronounced tails, several cosmic spherules also have microtails—much smaller extensions of melt that form sharp spiked projections, often composed exclusively of silicate glass (THMM318, THMM465, THMM531, THMM550, and THMM612 [Figs. 5C and 5D and given in the supplementary data]). Particles with microtails often have multiple protrusions spread randomly across their surface. Microtails have not previously been reported in cosmic spherules and this may be because subaerial Antarctic specimens are less likely to preserve these delicate features.

A single microtailed particle (THMM465) was selected for sectioning. In section view, however, the microtails were not present (Fig. 11D). Particle THMM465 (Fig. 11D) was initially classified as an S-type cosmic spherule; however, after sectioning, we reclassified this particle as a coarse-grained micrometeorite. It is therefore the only unmelted micrometeorite recovered in this study. The micrometeorite is dominated by a single mineral with an anhedral morphology and numerous branching melt veins that are spread throughout the crystal composed either of Fe-rich glass or containing Fe-rich dendrites (most likely magnetite). Several submicron rounded vesicles are also present in the crystal core. It is possible that the other four micrometeorites with microtails may also be unmelted micrometeorites, but we cannot be certain without sectioning.

DISCUSSION

Evaluating the Micrometeorite Mass Flux Using an Urban Rooftop Collection

Global flux estimates for the mass of micrometeorite material falling to Earth vary over three

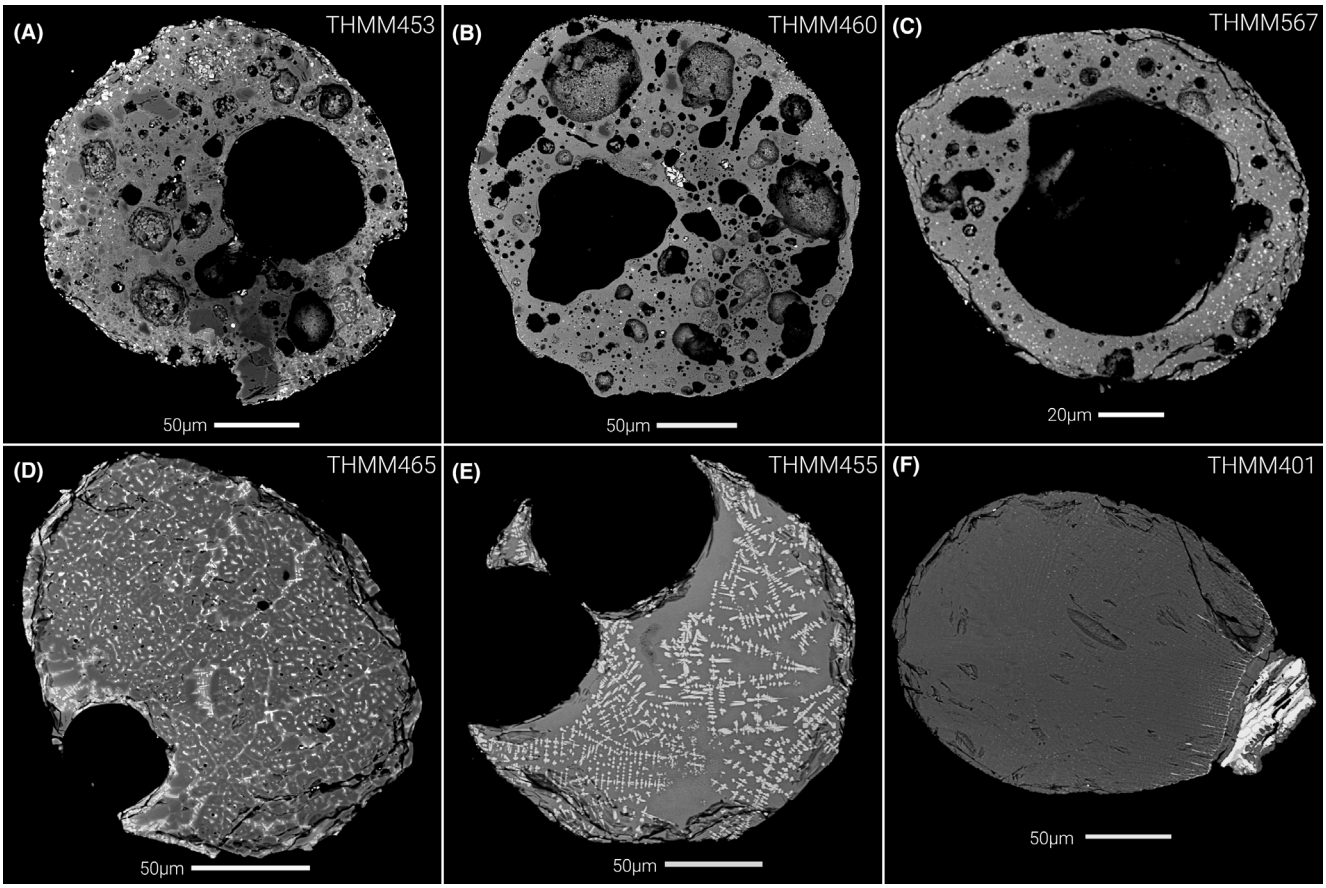

Fig. 11. Sectioned micrometeorite interiors imaged under SEM-BSE. Panels (A), (B), and (C) show fine-grained scoriaceous micrometeorites. They retain thin magnetite rims which enclose a vesicular matrix containing rare relict mineral grains (forsterite and/or Fe-sulfides) suspended in a glassy Fe-rich groundmass. Particle THMM567 (C) has a single large off-center vesicle, forming a "hollow" texture, it likely formed due to high spin rates during atmospheric entry (Genge 2017). Panel (D) shows particle THMM465 interpreted as an unmelted coarse-grained micrometeorite dominated by a single mineral and containing a network of melt veins. The external images of this particle revealed the presence of microtails. This micrometeorite is most likely a chondrule fragment that experienced a low degree of partial melting during atmospheric entry. Panel (E) shows a G-type micrometeorite and panel (F) shows an S-type micrometeorite which contains a large oval-shaped metal bead. The external image of this particle (THMM401 [Figs. 5M and 5N]) revealed the presence of an Fe-rich crust, while the sectioned interior shows Fe-rich melt that penetrated between olivine dendrites late in the particle's flight, after olivine had crystallized and before the Fe-rich melt cooled.

orders of magnitude. Disparities in the amount of infalling material estimated appear largely dependent on the data used. For example, space-based estimates derived from satellite observations of the Zodiacal Cloud (Carrillo-Sánchez et al. 2015), meteor showers (Dohnanyi 1972), or micrometeorite impacts into the Long-Duration Exposure Facility (LDEF; Love and Brownlee 1993) produce the largest flux figures, between 20,000 and 60,000 t yr^{-1}. Conversely, atmosphere and Earth-based estimates produce much lower flux values. Radar observations of the upper atmosphere produce dust flux estimates between 1600 and 2300 t yr^{-1} (Mathews et al. 2001), while calculations evaluating the abundance of micrometeorites in different collections arrive at values between 160 (±70) t yr^{-1} (Prasad et al. 2013) and 6400 (±1100) t yr^{-1} (Duprat et al. 2001), with most calculations favoring values around 1500 t yr^{-1} (see Suttle and Folco [2020] for a detailed analysis of previous flux estimates based on micrometeorite abundances). Finally, deep sea flux calculations, which measure the concentrations of extraterrestrial trace elements (Os and Ir) in marine sediments, also produce high values (37,000 ± 13,000 t yr^{-1}, Peucker-Ehrenbrink 1996). This disparity in flux estimates is largely due to atmospheric entry heating (Yiou et al. 1989). Rapid deceleration results in intense flash heating with many micrometeorites being vaporized. By comparing the abundance of micrometeorites recovered from sediment

traps against the influx of cosmic dust measured at the LDEF, Taylor et al. (1998) suggested that 90% of dust entering the Earth's atmosphere does not survive. This value is supported by numerical modeling experiments (Love and Brownlee 1991; Carrillo-Sánchez et al. 2015). Consequently, it appears that space-based fluxes or surface chemical analogs (using deep sea Os and Ir concentrations) sample close to the true value of the total dust flux, while micrometeorite collections sample only those particles that have survived entry.

The Meppen rooftop micrometeorite collection provides a new perspective on the mass flux of extraterrestrial material (that survives atmospheric entry). This is because previous mass flux estimates based on micrometeorite abundances have exclusively used Antarctic or deep sea collections with long accumulation ages (see Suttle and Folco 2020). For several of these sites, either the total area sampled and/or the accumulation window of the micrometeorite collection are poorly constrained—often with age uncertainties on the order of 1000s of years to millions of years. This is a particularly acute problem for the Transantarctic Mountain (TAM) micrometeorite collection, whose accumulation window is constrained between 800,000 and 2,300,000 years (Suttle and Folco 2020). Conversely, both the age and surface area of traps from Antarctic blue ice and snow have much better resolved parameters (e.g., Taylor et al. 1998; Dobrică et al. 2010).

Using each micrometeorite's average diameter (determined from BSE images), we calculated particle volumes and, assuming a fixed particle density of 2700 kg m^{-3} (Suttle and Folco 2020), we determined particle masses. The combined mass of the 315 micrometeorites is 0.00415 g (4.15×10^{-9} t). The total area of rooftop searched in this study is ~7500 m^2 and the rooftop age is 21 yr. This equates to a (local) flux value of 2.63×10^{-14} t m^{-2} yr^{-1}. Extrapolating to a global flux value gives 13.4 t yr^{-1}.

Our global micrometeorite mass flux estimate is anomalously small, being approximately two orders of magnitude less than previous estimates based on micrometeorite abundance data (which generally range between 1000 and 6500 t yr^{-1} [Suttle and Folco 2020]). The Meppen flux estimate is likely incorrect, despite both the site's surface area (7500 m^2) and accumulation window (age) being extremely well constrained. Instead, the anomalously low value is best explained as a product of significant micrometeorite loss from the rooftop. Most notably, this will arise due to the removal of particles via drainage systems (carried by rainwater), loss via annual cleaning to maintain the water drainage, and potentially also loss as particles are carried away in high winds. However, another factor that will have contributed to micrometeorite loss is the sediment processing and particle extraction protocol employed. Urban micrometeorite traps (rooftops, rain gutters, road sweepings, etc.) are sediment-rich, especially in comparison to Antarctic blue-ice, snow, and moraine. It is this huge quantity of terrestrial sediment that the extraterrestrial dust is mixed into that acts as a significant barrier to micrometeorite extraction. To overcome this problem requires processing techniques that concentrate micrometeorites at the expense of terrestrial sediment. Often researchers take advantage of micrometeorites' magnetic properties (magnetic separation using a Frantz separator or by passing a sheathed magnetic over or through a thin layer of dry sediment), their small size (sieving), and their higher (average) densities than most terrestrial particles (water suspension gravity settling) to concentrate micrometeorites.

In this study, we used all three sampling techniques: magnetic separation, sieving, and finally density separation. These processing steps resulted in a non-negligible loss of micrometeorites. For example, although most micrometeorites contain magnetic phases (notably magnetite, Fe-Ni-metal, chromite, and pyrrhotite), a small fraction of the population (often) contain no magnetic minerals. The V-type cosmic spherules (composed of silicate glass) are nonmagnetic (unless they also host an Fe-Ni-metal bead). As a result, they will always be missed in any technique that relies on magnetic extraction. Glassy V-type spherules make up approximately 18% of cosmic spherules in unbiased collections (Taylor et al. 2000). In contrast among both Jon Larsen's first micrometeorite finds reported in Genge et al. (2017a) and this population (Fig. 4), V-type spherules are significantly underrepresented. Correcting for the lack of V-types gives a mass flux of 16.7 t yr^{-1} and therefore has minimal effect on the total final flux value.

To better understand micrometeorite losses, we conducted searches of the discarded material. We analyzed a small aliquot (3% [470 g]) of the air-bound nonmagnetic sediment (Table 1) and identified 13 particles, all of which were magnetic—demonstrating that the magnetic separation technique used has limited efficiency. Upscaling to the whole discarded nonmagnetic sediment fraction implies that approximately 587 micrometeorites were missed at this stage. To investigate how sieving impacted loss, we searched the coarsest size fractions of sediment (>800 μm) and found several additional particles. All of these micrometeorites have sizes <800 μm, illustrating that sieving also introduces loss, consistent with the findings of Goderis et al. (2020). By contrast, the loss of micrometeorites during the density separation process

was mostly cancelled out by our later efforts to recover these missed particles—achieved by searching the decanted fraction (resulting in a further 19 micrometeorites, Table 1). As with almost all other micrometeorite studies, the smallest size fractions of micrometeorites (those <100 μm) were not primarily targeted, some will have been lost as part of the decanted fraction, and others will have been missed during optical searching of the sample because the selection criteria were not always recognizable for their size.

The loss of micrometeorites by weathering is unlikely to have played a significant role, given the exceptional preservation state of these particles (Figs. 5, 6, and 8), which show no evidence of mineral encrustation, generally contain unoxidized Fe-Ni-metal beads, well-preserved silicate crystals, and minimal evidence of etching affecting the exposed glass. By contrast, the often heavily weathered micrometeorites (Van Ginneken et al. 2016) found in deep sea (Blanchard et al. 1980; Prasad et al. 2013) and subaerial Antarctic collection sites (e.g., Larkman Nunatak [Genge et al. 2018]) show clear signs of dissolution, corrosion, and replacement.

In total, we estimate that approximately 15–30% of all the micrometeorites that were present on the rooftop (at the time of sampling) were recovered while further 70–85% were lost during sediment processing. It is difficult to better quantify the total loss of micrometeorites as a result of the above processing steps without performing a separate dedicated study on this topic. However, assuming a recovery rate of 15–30%, and assuming that the missed micrometeorites followed the same size distribution as the collected micrometeorites, the corrected global mass flux value for the Meppen rooftop lies between 43.8 and 87.7 t yr^{-1}. Since we expect that the missed micrometeorites may be preferentially biased toward smaller specimens, the corrected mass flux values given above are therefore upper estimates with the true value likely being lower than this. Even when accounting for the missed micrometeorites (due to our processing techniques) the mass flux values remain significantly below the global mass flux estimates based on other micrometeorite collection sites (Suttle and Folco 2020), we therefore conclude that factors apart from the micrometeorite concentration and the recovery methods employed remain the biggest source of loss—these factors are loss via water drainage, loss via annual cleaning works, and loss by strong winds. They remain the biggest problems limiting an accurate flux calculation in any urban rooftop site.

If future studies reattempt micrometeorite mass flux estimates, this study demonstrates that rooftop sites will need to be carefully selected to limit, as much as viable, micrometeorite loss via water drainage and loss by remedial rooftop cleaning. This could be achieved perhaps through the use of filtration systems and/or by continuous active magnetic extraction. Furthermore, current sampling techniques require improvement to maximize the recovering rate of micrometeorites from the roof sediment.

Size Distribution and Components of the Micrometeorite Flux

We compared the size–frequency distribution of our Meppen urban rooftop collection (Fig. 3) against both the Larkman Nunatak (Genge et al. 2018) and the TAM(65) collection (Suttle and Folco 2020). These sites are well-established subaerial Antarctic collections derived from blue-ice moraine and weathering cracks in exposed mountain tops (respectively). They have long accumulation ages exceeding 800,000 yr (Rochette et al. 2008; Suavet et al. 2009; Genge et al. 2018) in stark contrast to the Meppen rooftop age of just 21 yr.

Despite extreme differences between these collections, all three show similar size–frequency distributions. Micrometeorite abundances in both the Meppen and Larkman collections peak at ~150 μm. The TAM collection also has a smaller peak located at 150 μm and although its main peak is located at ~250 μm, the TAM65 trap is depleted in smaller particles (<200 μm) likely reflecting a site-dependent sorting process (Suttle and Folco 2020). All three sites also have several smaller peaks (in the Meppen data at 205 and 325 μm, in the Larkman collection at 235 and 295 μm, and in the TAM[65] trap at 235, 295, and 355 μm). Good agreement is seen between the smaller peak positions in the two Antarctic collections, while the smaller peaks in the Meppen data occur at different positions. We note that all three sites were processed with different cascade sieve sizes, and several different researchers, so sediment processing and human error are unlikely to have imparted a systematic effect on these distributions.

Previously Suttle and Folco (2020) suggested that multiple peaks within the micrometeorite flux imply several different sources (with distinct size distributions) that contribute to the dust flux reaching Earth. If this is the case, the similarity in the 150 μm peak position (seen in the Meppen and Larkman data) could indicate that this component has remained the dominant input over the last 800,000 yr; meanwhile, variations in the smaller peak positions would indicate variations in minor components that make up the micrometeorite flux over time.

Scoriaceous Micrometeorites among Urban Collections

Scoriaceous micrometeorites are particles that experienced partial melting during atmospheric entry (Genge et al. 2008). This constrains their peak temperatures to above the solidus and below the liquidus of chondritic materials (by contrast cosmic spherules are particles whose peak temperature exceeded the liquidus). A defining feature of both unmelted and ScMMs, but critically absent from cosmic spherules, is the presence of a magnetite rim (Genge et al. 2008). The magnetite forms during atmospheric entry by localized partial melting at the micrometeorite's margin. The resulting melt is Fe-enriched and subsequently experiences oxidation, cooling, and crystallization resulting in a paired (inner) igneous rim (composed of silicate glass) covered by a thin (typically <5 μm thick) shell of magnetite crystals (Toppani et al. 2001; Toppani and Libourel 2003; Genge 2006; Genge et al. 2008).

The absence of magnetite rims on cosmic spherules and their presence on ScMMs provide a clear diagnostic feature for easily discriminating one class of particles from the other. In this study, we identified eight particles that have at least a partial magnetite rim. In Fig. 6, we display six of these particles arranged as a series of panels (from Figs. 6A–R). Their order approximately reflects the continuum of properties displayed by micrometeorites as they evolve from ScMM to PO cosmic spherules. In general, irregular shapes are progressively replaced by increasingly (sub)spherical shapes while protrusions become less common. At the same time, the magnetite rim evolves from a thin but complete covering of tiny (~1–2 μm-sized) grains (as in THMM460 [Figs. 6A–C and 11B] and THMM567 [Figs. 6D–F and 11C]) to a thicker shell with larger (~5 μm-sized) euhedral grains (as in THMM566 [Figs. 6G–I] and THMM563 [Figs. 6J–L]). In particles that experienced more thermal processing magnetite grains are less common, ultimately exposing the silicate-rich mesostasis (as in THMM453 [Figs. 6M–O] and THMM363 [Figs. 6P–R]). Finally, in THMM354 (supplementary data in Hasse et al. 2021), no magnetite rim remains. This particle does, however, retain a high abundance of vesicles, indicating high internal porosities while also lacking other typical textural features of PO spherules (e.g., the exposed glassy mesostasis with suspended microphenocrysts).

Toppani et al. (2001) suggested that, as thermal processing advanced (reflecting either higher peak temperatures or longer duration heating), the (surface) melt layer evolved in composition from an Fe-rich melt to a more chondritic composition (addition of more Si, Mg, and Al). This occurs because Fe-rich phases in the unmelted precursor micrometeorite (such as ferrihydrite, Fe-cronstedtite, and tochilinite) have relatively low melting points while Mg-, Si-, and Al-rich phases (such as olivine, pyroxene, anorthite, Mg-serpentine, and saponite) tend to have higher melting points. As a result, small degrees of partial melting favor Fe-enrichment but as partial melting transitions into complete melting, the early Fe-enrichment is passively diluted. Iron then crystallizes both as magnetite and as FeO-rich olivine, and in micrometeorites, this is observed as a change from magnetite rims on unmelted and ScMMs to silicate-dominated mesostasis in cosmic spherules.

The discovery of ScMMs (and particles transitional between scoriaceous and PO textural types) among urban micrometeorite collections is notable. Early collection efforts reported recovering only cosmic spherules (e.g., Genge et al. 2017a; Larsen 2017, 2019; Blake et al. 2018; Esposito et al. 2020). However, this study alongside the recent finds of Larsen and Kihle (2020) and Peterson (2020) demonstrates that unmelted and partially melted representatives can be successfully recovered from urban environments. Since analysis of unmelted/ScMMs allows for a more direct investigation of the micrometeorite's parent body geology, this discovery enhances the research potential of urban micrometeorite collections.

Metal/Sulfide Beads, PGNs, and Surface Wetting Events in Cosmic Spherules

Upon melting, sulfur (and phosphorus) bond with siderophile elements (Fe, Ni, Co, and PGEs) forming an immiscible Fe-rich liquid that is suspended in the silicate melt (Brownlee et al. 1984; Genge and Grady 1998; Palme 2008; Taylor et al. 2011; Helmy et al. 2020). Often this Fe-rich liquid coalesces to form a single bead (e.g., THMM401, Figs. 5M and 11F), although particles containing multiple small beads are commonly observed (e.g., THMM355 [see supplementary data in Hasse et al. 2021]). They may reflect particles with spinning flight histories whose centrifugal forces prevented bead coalescence (Dionnet et al. 2020).

Owing to the immiscible nature of the two fluids and the rapid deceleration of the particle, which acts to emphasize density contrasts (Genge et al. 2016), high-density beads move to the edge of the cosmic spherule and are often located at the leading front (or "head") of the particle. At this point, the bead can either escape the particle in an ejection event (Brownlee et al. 1984; Bi et al. 1993; Alexander et al. 2002; Genge et al. 2008), flow out of the cavity it is held in, wetting the particle's surface (Taylor et al. 2000, 2011; Alexander et al. 2002) —as observed here in nine particles (THMM317,

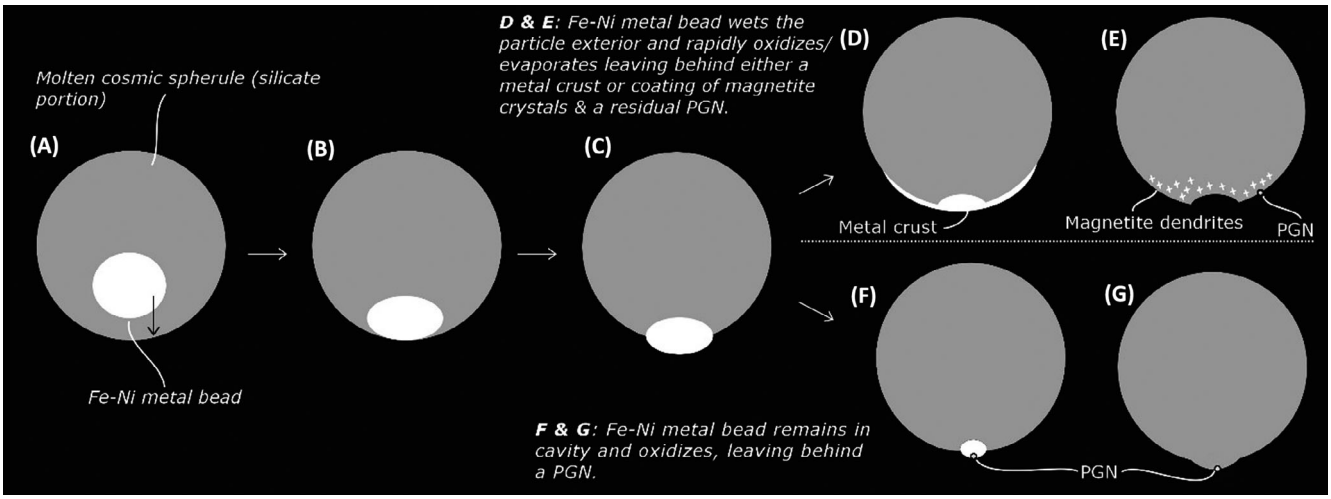

Fig. 12. A–G) Diagram illustrating the evolution of Fe-Ni-S beads in cosmic spherules during atmospheric entry. Gray denotes silicate melt, white denotes an Fe-Ni(-S) bead, and a smaller gold colored circle with a black outline denotes a PGN. This cartoon details how beads become exposed at the particle perimeter (A–C) and then either cool and crystallize (leaving particles like C) or continue to oxidize and evaporate leaving PGNs (as in F and G). Alternatively, if the bead flows out over the particle's exterior (D), then the spherule may cool and crystallize preserving an Fe-rich metallic crust (D), or this may continue to evaporate and oxidize leaving a high-density region of magnetite crystals, with or without a PGN (E).

THMM326, THMM328, THMM374, THMM401 [shown in Figs. 5M–P and 11F], THMM405, THMM418, THMM432, and THMM516), or remain in its cavity and continue to oxidize and evaporate (Fig. 12 [pathway shown in panel progression C→F→G]). However, once exposed at the micrometeorite's perimeter, volatile sulfur (and phosphorous) in the bead preferentially boil off at a faster rate than Fe and Ni. This results in a progressively metal-rich composition (Taylor et al. 2011).

Assuming the bead remains in its cavity, further heating drives progressive oxidization and evaporation. Oxidation converts metals into positively charged divalent ions that can then partition back into the silicate melt. However, since Fe has a higher oxidation potential than Ni, Fe preferentially oxidizes leaving the bead progressively enriched in Ni as it decreases in size (Brownlee et al. 1984; Bi et al. 1993). Platinum group elements are even more resistant to both oxidation and evaporation than Ni (Palme 2008), thus as the metal bead decreases in size, PGEs are passively concentrated (Brownlee et al. 1984). Ultimately, PGNs can be considered residues left over after evaporation and oxide growth (Brownlee et al. 1984; Taylor et al. 2000; Rudraswami et al. 2014).

Platinum group nuggets were first reported by Brownlee et al. (1984) in I-type and by Bonté et al. (1987) in S-type cosmic spherules. Later, Rudraswami et al. (2014) analyzed large numbers of PGNs in I-, G-, and S-type spherules. In silicate-dominated S-types, PGNs are exposed on the particle exterior (reflecting their immiscibility in the silicate melt) and range in size between 0.5 and 3.0 μm (26 nuggets). This is in accordance with the PGNs identified in this study, which were found on particle exteriors and vary in size from 0.6 to 1.6 μm (8 nuggets [plus one additional nugget identified from a sectioned interior]). Rudraswami et al. (2014) also calculated the apparent frequency of PGNs and arrived at values of 7.9% (I-types), 8.8% (G-types), and 3.3% (S-types). Our data show similar abundances for S-type cosmic spherules (2.5%); however, because we analyzed only a single hemisphere on each particle, we may expect double this value, with PGNs expected on approximately 5.0% of S-type cosmic spherules.

Metal abundances in the Meppen PGNs have chondritic profiles (Fig. 9) that fall within the compositional range of previously published PGNs found in micrometeorites (Fig. 10). The more refractory elements (Os, Ru, Pt, and Rh) have chondritic concentrations varying between 0.2–2.0× CI values, while the more volatile metals (notably Pd) show clear depletions (in some instances down to 0.001× CI values). This attests to the effects of flash heating during atmospheric entry. Interestingly however, in a single spherule (THMM516 [Fig. 8H]), both Ni and Pd are not depleted (Fig. 9). The host micrometeorite is a CC spherule. Its PGN is located on a region of the particle's surface that contains a high density of magnetite crystals and is near a large ellipsoid-shaped hollow—strongly indicating the site where a former Fe-rich bead escaped from the particle in either an ejection

event or flowed out along the surface of the spherule wetting the exterior. A wetting event is more likely than an ejection event since ejection would have carried away the PGN along with the Fe-Ni bead.

Other particles in this collection show evidence of beads smearing out across their external surface (e.g., THMM401 shown in Figs. 5M–P and 11F). These Fe-rich coatings do not extend over the entire particle but are instead limited to a small region surrounding their source bead. Once exposed on the micrometeorite's surface, they would rapidly lose any remaining volatile sulfur (and phosphorous) that was held in the melt, leaving a metallic liquid. Supporting this prediction, the measured chemical compositions of Fe-rich coverings (Table 4) contain only trace quantities (<1 wt%) of phosphorus and sulfur, in contrast to their source metal beads, which show slightly higher average combined sulfur/phosphorus contents of 2.1 wt% (Table 4). Such low S/P abundances in the metallic coverings attest to the former presence of dissolved volatiles while also demonstrating that they have largely boiled off into Earth's atmosphere during entry. We also note that Fe-rich surface coverings are systematically depleted in Ni relative to their source beads (as shown in Table 4). Such depletions in the surface coatings may reflect redox controlled fractionation of Ni into the less oxidized metal bead (a process that can occur in a matter of seconds as demonstrated from hypervelocity impact experiments [Ebert et al. 2014]).

Table 4. Compositions of Fe-rich coatings that partially cover the external surface on some micrometeorites. These coverings are associated with Fe-Ni(-S) beads (whose measured compositions are also given). Compositions were determined by EDS. Owing to beam penetration, some Si, Al, and Mg present in the silicate fraction below the Fe-rich coating was detected. We removed these elements from the analysis and renormalized the data. Compositions are given as wt% and quoted to one decimal place.

Particle	Analy. Location	Fe	Ni	S	P	Total
THMM317	Surface covering	98.3	0.2	b.d.l.	1.5	100.0
THMM326		95.0	3.4	1.1	0.5	100.0
THMM328		99.4	0.3	b.d.l.	0.3	100.0
THMM401		98.5	0.8	0.3	0.3	100.0
THMM418		97.9	1.4	b.d.l.	0.6	100.0
THMM432		99.5	0.1	b.d.l.	0.4	100.0
Average		98.1	1.0	0.2	0.6	100.0
THMM317	Source metal	91.8	2.0	0.4	5.8	100.0
THMM326	bead	80.0	19.0	0.9	0.1	100.0
THMM328		98.5	0.7	b.d.l.	0.8	100.0
THMM401		91.4	6.7	1.1	0.8	100.0
THMM432		98.6	0.9	0.2	0.3	100.0
Average		92.1	5.9	0.5	1.6	100.0

b.d.l. = detection limit. All the Fe-rich coverings contain trace phosphorus and several also have trace sulfur. Note that Ni abundances are systematically higher in the source beads when compared against the surface coverings; this could reflect preferential redox partitioning of Ni into the less oxidized bead phase.

After a wetting event, a thin Fe-rich melt layer covering the particle's exterior is likely to experience further oxidation and evaporation. Evidence of this can be seen in THMM516 (Fig. 8H)—the region surrounding the hollow cavity (and in which the PGN is located) contains a locally high density of cruciform magnetite crystallites; they potentially formed by the oxidation of an Fe-rich melt layer. Furthermore, because the PGN in THMM516 has preserved chondritic abundances of volatile Pd, this nugget may have been protected from severe heating. The presence of an Fe-rich envelope covering the nugget, therefore, presents a plausible explanation for the observed anomalous composition (Fig. 12).

Among the Meppen collection, we observe eight particles with direct evidence of Fe-rich partial coatings surrounding a source cavity. They have crystallized as Fe-Ni metal (and not magnetite [Table 4]), indicating that wetting followed by rapid quench cooling may be more common than oxidation and the formation of a high-density magnetite coverings. Furthermore, since the survival of a thin Fe-rich melt on the micrometeorite exterior is necessarily short (rapidly evaporating into Earth's atmosphere), many more cosmic spherules may have experienced a wetting but no longer preserve (direct) evidence. Based on the abundance of particles with direct evidence of surface wetting, we argue that at least 3% of S-type cosmic spherules experience bead wetting during atmospheric entry. This process has historically been overlooked but is likely to play a role in controlling cosmic spherule bulk chemistry, texture, and the survival of some phases (e.g., PGNs).

Finally, we note that the other PGNs found on the surfaces of S-type micrometeorites in this study show no association with metal beads but instead are located at the center of a shallow cone-shaped mound on the cosmic spherule's exterior and have radiating silicate crystals (Figs. 8B, 8C, and 8I) or radiating magnetite crystals (Fig. 8D). These textures show that PGNs acted as nucleation points during crystallization. If all PGNs were previously held within a host Fe-Ni(-S) bead, then the location and abundance of PGNs in a micrometeorite may indicate the former existence of beads that have since oxidized and evaporated.

Implications and Outlook

Urban micrometeorites offer an exciting new resource for the planetary science community. Their exceptional preservation state (minimally affected by terrestrial weathering), relative ease of extraction (in comparison to deep sea or Antarctic collections), and huge site potential (with almost any rooftop site acting as a micrometeorite trap) make urban micrometeorites highly accessible both to the research community but also to citizen science and educational projects as well as to interested amateurs keen to start their own collections.

Increasingly new urban micrometeorite collections are being reported, as evidenced by the growing number of publications on this topic (Genge et al. 2017a; Larsen 2017, 2019; Blake et al. 2018; Esposito et al. 2020; Larsen and Kihle 2020; Peterson 2020). However, we stress that readers interested in collecting their own particles remain cautious and ensure due diligence when conducting positive micrometeorite identification. At a minimum, a representative subset of the candidate particles should be analyzed not only under optical microscope but also under SEM with supporting chemical data (EDS). Ideally this should include sectioning and analysis of their internal textures for some particles. It is essential that the criteria outlined in Genge et al. (2008, 2017a, 2017b) and summarized here in the Identifying Micrometeorites section are used as a guide. As demonstrated in Larsen (2017), there are numerous "micrometeor-wrongs"—anthropogenic particles with similar characteristics that can mislead the uninformed. The requirement for SEM is unfortunate as this represents a barrier to citizen science or school-based projects. Occasionally, this has been overcome by collaboration with researchers as in Esposito et al. (2020).

Beyond collection and characterization, urban micrometeorites have some distinct advantages over particles derived from other collections. In comparison to the more weathered micrometeorites typically recovered from subaerial Antarctic sites and deep-sea collections, urban micrometeorites have near pristine external surfaces meaning that textural classification can be performed solely on the basis of SEM-BSE and/or optical images (as in this study) without the requirement for destructive sectioning, time-consuming μCT (Van Ginneken et al. 2017), or minimally destructive focused ion-beam milling to expose the particle interior (Feige et al. 2018). This means that rapid nondestructive classification can be performed (with a high degree of certainty) and the classified micrometeorites can then be diverted for whole-particle destructive analyses, particularly those which benefit from the maximum possible mass of micrometeorite—for example, laser-fluorination O-isotope mass spectrometry (Goderis et al. 2020) or cosmogenic ^{26}Al and ^{10}Be measurements (Feige et al. 2018). Given these advantages, combined with their exceptionally young terrestrial residence times, urban micrometeorites are ideally suited for implanted cosmogenic nuclide studies. This is because cosmic ray exposure age dating studies also benefit from precisely known terrestrial ages that otherwise add uncertainty to the exposure record of the sample (Eugster et al. 2006). We anticipate that the role of urban micrometeorites as a scientific resource will continue to expand over the coming decades as their advantages continue to be recognized by the community.

CONCLUSIONS

We investigated the abundance of micrometeorites on a single rooftop of an industrial building in Meppen, Germany. The resulting micrometeorite collection (containing 315 particles with sizes between 55 and 515 μm) was used in the first mass flux calculation from an urban micrometeorite collection. This produced an anomalously low flux value of 13.4 t yr^{-1}, despite strong constraints on the collection sites age (21 yr) and total area (<8400 m^2). We attribute this low value to micrometeorite loss, primarily via the rooftop's drainage system and by removal of dust during annual cleaning, with further loss due to the sediment processing techniques used. This result emphasizes the need for careful selection or bespoke design of a rooftop site that minimizes micrometeorite loss and for improvements in micrometeorite concentration techniques.

Analyzing the collection's size–frequency distribution demonstrates a mass peak at ~150 μm, consistent with the mass peak at the Larkman Nunatak collection site in Antarctica, potentially suggesting minimal change in the component sources of the micrometeorite flux over the last 800,000 yr.

The Meppen rooftop collection further demonstrates the viability of successful micrometeorite recovery from urban sites (after the works of Genge et al. 2017a; Larsen 2017, 2019; Blake et al. 2018; Peterson 2020). We hope that this study will act as a pilot resource for future researchers, interested amateurs, citizen scientists, or student-led science projects by providing a template from which other parties may copy. Furthermore, we anticipate that the role of urban micrometeorites as a scientific resource is likely to grow owing to the ease of recovery and numerous potential recovery sites as well as the research benefits that they can provide (i.e., short terrestrial ages minimally affected by weathering which preserve delicate structures [i.e., microtails] and/or rare phases [i.e., PGNs]).

We also analyzed the chemical and textural characteristics of selected particles in the Meppen collection, exploring two main aspects:

1. ***The transition from partially melted to completely melted micrometeorites***: We analyzed several particles that span the continuum between scoriaceous and PO cosmic spherules. The defining feature that distinguishes (unmelted and) partially melted micrometeorites from cosmic spherules is the presence of a magnetite rim. Even in particles with near-spherical shapes (and thus high degrees of partial melting), the presence of a magnetite rim is clear indication of scoriaceous classification. The Fe-rich melt that produces a magnetite rim is progressively "diluted" as partial melting evolves toward complete melting. This is seen in micrometeorites as evolution from a thin but complete covering of magnetite crystallites to a sparse covering of larger grains that are ultimately replaced by silicate-dominated mesostasis.
2. ***The evolution of Fe-Ni-S beads***: Many cosmic spherules contain metal or Fe-Ni-S beads. Commonly they are exposed on the particle's outer surface. The process of metal bead ejection is well described, while the escape of beads from their cavities resulting in wetting of the micrometeorite exterior surface is less well known. In this collection, 3% of particles preserve direct evidence of this wetting process. However, many more particles likely experienced wetting but do not preserve evidence of this due to rapid evaporation of the thin Fe-rich melt layer. We identified a single micrometeorite containing a PGN, located close to a hollow cavity and within a region on the cosmic spherule's exterior containing a dense covering of magnetite dendrites. Unusually for micrometeorites, the PGN in this particle preserved chondritic abundances of volatile Pd. We suggest that the combined textural and chemical features of this micrometeorite are explainable as a product of surface wetting by an S-bearing Fe-Ni-rich melt which later evaporated and oxidized. This process shielded the PGN for high peak temperatures, preserving Pd from evaporation, while forming a region of locally dense magnetite crystals on the particle's surface.

Acknowledgments—MDS was funded by the Science and Technology Facilities Council (STFC), UK, through grant number ST/R000727/1—*The geological history of water-rich asteroids*. The Albers family (owner of the furniture store) kindly granted access to the building roof for this study. We thank Susan Taylor and Don Brownlee for their helpful comments and suggestions during the review process. Open Access funding enabled and organized by Projekt DEAL.

Editorial Handling—Dr. Donald Brownlee

REFERENCES

Alexander C. M. O'D., Taylor S., Delaney J. S., Ma P., and Herzog G. F. 2002. Mass-dependent fractionation of Mg, Si, and Fe isotopes in five stony cosmic spherules. *Geochimica et Cosmochimica Acta* 66:173–183.

Beckerling W. and Bischoff A. 1995. Occurrence and composition of relict minerals in micrometeorites from Greenland and Antarctica—Implications for their origins. *Planetary and Space Science* 43:435–449.

Bi D., Morton R. D., and Wang K. 1993. Cosmic nickel-iron alloy spherules from Pleistocene sediments, Alberta, Canada. *Geochimica et Cosmochimica Acta* 57:4129–4136.

Blake M., McKee J., Statom R., Qiu C., and Menapace F. 2018. Evaluating strategies to collect micrometeorites from rainwater for citizen scientists. *Journal of Astronomy & Earth Sciences Education* 5:151–160.

Blanchard M. B., Brownlee D. E., Bunch T. E., Hodge P. W., and Kyte F. T. 1980. Meteoroid ablation spheres from deep-sea sediments. *Earth and Planetary Science Letters* 46:178–190.

Bonté P. H., Jéhanno C., Maurette M., and Brownlee D. E. 1987. Platinum metals and microstructure in magnetic deep sea cosmic spherules. *Journal of Geophysical Research* 92:E641–E648.

Brownlee D. E., Bates B., and Beauchamp R. H. 1983. Meteor ablation spherules as chondrule analogs. In King, E. A. (Ed.) *Chondrules and their origins*. Houston, Texas: Lunar and Planetary Institute. pp. 10–25.

Brownlee D. E., Bates B., and Wheelock M. M. 1984. Extraterrestrial platinum group nuggets in deep-sea sediments. *Nature* 309:693–695.

Brownlee D. E., Bates B., and Schramm L. 1997. The elemental composition of stony cosmic spherules. *Meteoritics & Planetary Science* 32:157–175.

Buddhue J. D. 1950. *Meteoritic dust (No. 2)*. Albuquerque, New Mexico: University of New Mexico Press.

Carrillo-Sánchez J. D., Plane J. M. C., Feng W., Nesvorný D., and Janches D. 2015. On the size and velocity distribution of cosmic dust particles entering the atmosphere. *Geophysical Research Letters* 42:6518–6525.

Cordier C., van Ginneken M., and Folco L. 2011. Nickel abundance in stony cosmic spherules: Constraining precursor material and formation mechanisms. *Meteoritics & Planetary Science* 46:1110–1132.

De Hoog C.-J., Gall L., and Cornell D. H. 2010. Trace-element geochemistry of mantle olivine and application to mantle petrogenesis and geothermobarometry. *Chemical Geology* 270:196–215.

Dionnet Z., Suttle M. D., Longobardo A., Rotundi A., Folco L., Della Corte V., and King A. 2020. X-ray computed tomography: Morphological and porosity characterization of giant Antarctic micrometeorites. *Meteoritics & Planetary Science* 55:1581–1599.

Dobrică E., Engrand C., Duprat J., Gounelle M., Leroux H., Quirico E., and Rouzaud J. N. 2009. Connection between micrometeorites and Wild 2 particles: From Antarctic

snow to cometary ices. *Meteoritics & Planetary Science* 44:1643–1661.

Dobrică E., Engrand C., Duprat J., and Gounelle M. 2010. A statistical overview of concordia Antarctic micrometeorites (abstract #5213). *Meteoritics & Planetary Science Supplement* 73.

Dobrică E., Engrand C., Leroux H., Rouzaud J. N., and Duprat J. 2012. Transmission electron microscopy of CONCORDIA ultracarbonaceous Antarctic micrometeorites (UCAMMs): Mineralogical properties. *Geochimica et Cosmochimica Acta* 76:68–82.

Dohnanyi J. S. 1972. Interplanetary objects in review: Statistics of their masses and dynamics. *Icarus* 17:1–48.

Duprat, J., Dobrică, E., Engrand, C., Aléon, J., Marrocchi, Y., Mostefaoui, S., Melbom, A., Leroux, H., Rouzaud, J. N., Gounelle, M., and Robert, F. 2010. Extreme deuterium excesses in ultracarbonaceous micrometeorites from central Antarctic snow. *Science* 328:742–745.

Duprat J., Maurette M., Engrand C., Matraj G., Immel G., Hammer C., Gounelle M., and Kurat G. 2001. An estimation of the contemporary micrometeorite flux obtained from surface snow samples collected in central Antarctica. *Meteoritics & Planetary Science Supplement* 36: A52.

Duprat J., Engrand C., Maurette M., Kurat G., Gounelle M., and Hammer C. 2007. Micrometeorites from central Antarctic snow: The CONCORDIA collection. *Advances in Space Research* 39:605–611.

Ebert M., Hecht L., Deutsch A., Kenkmann T., Wirth R., and Berndt J. 2014. Geochemical processes between steel projectiles and silica-rich targets in hypervelocity impact experiments. *Geochimica et Cosmochimica Acta* 133:257–279.

Engrand C., McKeegan K. D., and Leshin L. A. 1999. Oxygen isotopic compositions of individual minerals in Antarctic micrometeorites: Further links to carbonaceous chondrites. *Geochimica et Cosmochimica Acta* 63:2623–2636.

Esposito M., Souhrada K., Garland E., Kroll M., Bolen R., Hernandez V., Kaczmarek J., Meisel D., Swiss A., Northrup P., Stojanoff V., Thieme J., and Perez A. 2020. Characterization of potential micrometeorites by synchrotron analysis. *Geosciences* 10:275.

Eugster O., Herzog G. F., Marti K., and Caffee M. W. 2006. Irradiation records, cosmic-ray exposure ages, and transfer times of meteorites. *Meteorites and the early solar system II*, edited by Lauretta D. S. and McSween H. Y. Jr. Tucson, Arizona: The University of Arizona Press. pp. 829–851.

Feige J., Airo A., Berger D., Genge M. J., Nissen J., Sager C., and Suttle M. D. 2018. A methodological approach for identifying micrometeorites for subsequent measurement of cosmogenic 26Al and 10Be. 15th International Symposium on Nuclei in the Cosmos, June 24–29, Nazionali del Gran Sasso, Italy.

Folco L. and Cordier C. 2015. Micrometeorites. *EMU Notes in Mineralogy* 15:253–297.

Genge M. J. 2006. Igneous rims on micrometeorites. *Geochimica et Cosmochimica Acta* 70:2603–2621.

Genge M. J. 2017. Vesicle dynamics during the atmospheric entry heating of cosmic spherules. *Meteoritics & Planetary Science* 52:443–457.

Genge M. J. and Grady M. M. 1998. Melted micrometeorites from Antarctic ice with evidence for the separation of immiscible Fe-Ni-S liquids during entry heating. *Meteoritics & Planetary Science* 33:425–434.

Genge M. J., Engrand C., Gounelle M., and Taylor S. 2008. The classification of micrometeorites. *Meteoritics & Planetary Science* 43:497–515.

Genge M. J., Suttle M., and Van Ginneken M. 2016. Olivine settling in cosmic spherules during atmospheric deceleration: An indicator of the orbital eccentricity of interplanetary dust. *Geophysical Research Letters* 43:10,646–10,653.

Genge M. J., Larsen J., Van Ginneken M., and Suttle M. D. 2017a. An urban collection of modern-day large micrometeorites: Evidence for variations in the extraterrestrial dust flux through the Quaternary. *Geology* 45:119–122.

Genge M. J., Davies B., Suttle M. D., van Ginneken M., and Tomkins A. G. 2017b. The mineralogy and petrology of I-type cosmic spherules: Implications for their sources, origins and identification in sedimentary rocks. *Geochimica et Cosmochimica Acta* 218:167–200.

Genge M. J., van Ginneken M., Suttle M. D., and Harvey R. P. 2018. Accumulation mechanisms of micrometeorites in an ancient supraglacial moraine at Larkman Nunatak, Antarctica. *Meteoritics & Planetary Science* 53:2051–2066.

Goderis S., Soens B., Huber M. S., McKibbin S., van Ginneken M., Van Maldeghem F., Debaille V., Greenwood R. C., Franchi I. A., Cnudde V., Van Malderen S., Vanhaecke F., Koeberl C., Topa D., and Claeys P. 2020. Cosmic spherules from Widerøefjellet, Sør Rondane Mountains (East Antarctica). *Geochimica et Cosmochimica Acta* 270:112–143.

Gounelle M., Engrand C., Maurette M., Kurat G., McKeegan K. D., and Brandstatter F. 2005. Small Antarctic micrometeorites: A mineralogical and in situ oxygen isotope study. *Meteoritics & Planetary Science* 40:917–932.

Handy R. L. and Davidson D. T. 1953. On the curious resemblance between fly ash and meteoritic dust. *Proceedings of the Iowa Academy of Science* 60:373–379.

Hasse T. 2020. Urbane Mikrometeorite. Available at: www.micrometeorites.org

Hasse T., Hecht L., and Suttle M. D. 2021. Light-optical, back scatter electron images, and bulk chemical data of micrometeorites from an urban roof top at Meppen, Germany. Data Publisher: Museum für Naturkunde Berlin (MfN)—Leibniz Institute for Evolution and Biodiversity Science. https://doi.org/10.7479/506e-tk93.

Helmy H. M., Ballhaus C., Fonseca R. O., and Leitzke F. P. 2020. Concentrations of Pt, Pd, S, As, Se and Te in silicate melts at sulfide, arsenide, selenide and telluride saturation: Evidence of PGE complexing in silicate melts? *Contributions to Mineralogy and Petrology* 175:1–14.

Jarosewich E., Nelen J. A., and Norberg J. A. 1980. Reference samples for electron microprobe analysis. *Geostandards and Geoanalytical Research* 4:43–47.

Khisina N. R., Badyukov D. D., and Wirth R. 2016. Microtexture, nanomineralogy, and local chemistry of cryptocrystalline cosmic spherules. *Geochemistry International* 54:68–77.

Kohout, T., Kallonen, A., Suuronen, J. P., Rochette, P., Hutzler, A., Gattacceca, J., Badjukov, D. D., Skala, R., Böhmová, V., and Čuda, J. 2014. Density, porosity, mineralogy, and internal structure of cosmic dust and alteration of its properties during high-velocity atmospheric entry. *Meteoritics & Planetary Science* 49:1157–1170.

Kurat G., Koeberl C., Presper T., Brandstätter F., and Maurette M. 1994. Petrology and geochemistry of Antarctic micrometeorites. *Geochimica et Cosmochimica Acta* 58:3879–3904.

Larsen J. 2017. *In search of stardust: Amazing micrometeorites and their terrestrial imposters*. McGregor, MN: Voyageur Press.

Larsen J. 2019. *On the trail of Stardust: The guide to finding micrometeorites: Tools, techniques, and identification*. McGregor, MN: Voyageur Press.

Larsen J. and Kihle J. B. 2020. *Atlas of micrometeorites, a systematic classification in color photography*. Arthaus DGB, 318 p. ISBN:978-82-93805-00-7.

Lodders K. and Fegley B. 1998. *The planetary scientist's companion*. Oxford University Press on Demand.

Love S. G. and Brownlee D. E. 1991. Heating and thermal transformation of micrometeoroids entering the Earth's atmosphere. *Icarus* 89:26–43.

Love S. G. and Brownlee D. E. 1993. A direct measurement of the terrestrial mass accretion rate of cosmic dust. *Science* 262:550–553.

Mathews J. D., Janches D., Meisel D. D., and Zhou Q. H. 2001. The micrometeoroid mass flux into the upper atmosphere: Arecibo results and a comparison with prior estimates. *Geophysical Research Letters* 28:1929–1932.

Maurette M., Olinger C., Michel-Levy M. C., Kurat G., Pourchet M., Brandstätter F., and Bourot-Denise M. 1991. A collection of diverse micrometeorites recovered from 100 tonnes of Antarctic blue ice. *Nature* 351:44–47.

Micrometeorites—The Cosmic Treasure of Berlin Roofs. 2019. Available at: https://www.museumfuernaturkunde.berlin/en/science/berlin-collects-cosmic-dust

Murray J. and Renard A. F. 1891. Report on deep-sea deposits based on the specimens collected during the voyage of HMS Challenger in the years 1872 to 1876. HM Stationery Office. pp. 327–336.

Murrell M. T., Davis P. A. Jr., Nishiizumi K., and Millard H. T. Jr. 1980. Deep-sea spherules from Pacific clay: Mass distribution and influx rate. *Geochimica et Cosmochimica Acta* 44:2067–2074.

Nesvorný D., Bottke W. F., Levison H. F., and Dones L. 2003. Recent origin of the solar system dust bands. *The Astrophysical Journal* 591:486.

Nesvorný D., Vokrouhlický D., Bottke W. F., and Sykes M. 2006. Physical properties of asteroid dust bands and their sources. *Icarus* 181:107–144.

Newbury D. E. and Ritchie N. W. 2013. Is scanning electron microscopy/energy dispersive X-ray spectrometry (SEM/EDS) quantitative? *Scanning* 35:141–168.

Nininger H. H. 1941. Collecting small meteoritic particles. *Contributions of the Society for Research on Meteorites* 2:258–260.

Noguchi T., Ohashi N., Tsujimoto S., Mitsunari T., Bradley J. P., Nakamura T., Toh S., Stephan T., Iwata N., and Imae N. 2015. Cometary dust in Antarctic ice and snow: Past and present chondritic porous micrometeorites preserved on the Earth's surface. *Earth and Planetary Science Letters* 410:1–11.

Nordenskiöld N. A. E. 1874. On the cosmic dust which falls on the surface of the Earth with the atmospheric precipitation. *The Philosophical Magazine* 48:546–547.

Osawa T., Nageo K., Noguchi T., Nakazawa A., and Mikada J. I. 2003. Remnant extraterrestrial noble gases in Antarctic cosmic spherules. *Antarctic Meteorite Research* 16:196–219.

Palme H. 2008. Platinum-group elements in cosmochemistry. *Elements* 4:233–238.

Peterson S. 2020. Welcome to the search for Micrometeorites. Available at: https://micro-meteorites.com/

Peucker-Ehrenbrink B. 1996. Accretion of extraterrestrial matter during the last 80 million years and its effect on the marine osmium isotope record. *Geochimica et Cosmochimica Acta* 60:3187–3196.

Prasad M. S., Rudraswami N. G., and Panda D. K. 2013. Micrometeorite flux on Earth during the last ~50,000 years. *Journal of Geophysical Research: Planets* 118:2381–2399.

Rochette P., Folco L., Suavet C., Van Ginneken M., Gattacceca J., Perchiazzi N., Braucher R., and Harvey R. P. 2008. Micrometeorites from the Transantarctic Mountains. *Proceedings of the National Academy of Sciences* 105:18,206–18,211.

Rudraswami N. G., Parashar K., and Shyam Prasad M. 2011. Micrometer-and nanometer-sized platinum group nuggets in micrometeorites from deep-sea sediments of the Indian Ocean. *Meteoritics & Planetary Science* 46:470–491. https://doi.org/10.1111/j.1945-5100.2011.01169.x.

Rudraswami N. G., Prasad M. S., Plane J. M. C., Berg T., Feng W., and Balgar S. 2014. Refractory metal nuggets in different types of cosmic spherules. *Geochimica et Cosmochimica Acta* 131:247–266.

Salge T., Tagle R., Hecht L., Ferriere L., Ball A. D., Kearsley A. T., Smith C., and Jones C. 2014. Advanced EDS and μXRF analysis of Earth and planetary materials using spectrum imaging, computer-controlled SEM and an annular SDD. *Microscopy and Microanalysis* 20:1716–1717.

Schmidt R. A. 1965. *A survey of data on microscopic extraterrestrial particles*, vol. 2719. Washington, D.C.: National Aeronautics and Space Administration.

Steele I. M. 1992. Olivine in Antarctic micrometeorites: Comparison with other extraterrestrial olivine. *Geochimica et Cosmochimica Acta* 56:2923–2929.

Stuart F. M., Harrop P. J., Knott S., and Turner G. 1999. Laser extraction of helium isotopes from Antarctic micrometeorites: Source of He and implications for the flux of extraterrestrial 3He to earth. *Geochimica et Cosmochimica Acta* 63:2653–2665.

Suavet C., Rochette P., Kars M., Gattacceca J., Folco L., and Harvey R. P. 2009. Statistical properties of the Transantarctic Mountains (TAM) micrometeorite collection. *Polar Science* 3:100–109.

Suttle M. D. and Folco L. 2020. The extraterrestrial dust flux: Size distribution and mass contribution estimates inferred from the transantarctic mountains (TAM) micrometeorite collection. *Journal of Geophysical Research: Planets* 125:2019JE006241.

Suttle M. D., Folco L., Genge M. J., Russell S. S., Najorka J., and Van Ginneken M. 2019. Intense aqueous alteration on C-type asteroids: Perspectives from giant fine-grained micrometeorites. *Geochimica et Cosmochimica Acta* 245:352–373.

Suttle M. D., Folco L., Genge M. J., Franchi I. A., Campanale F., Mugnaioli E., and Zhao X. 2021. The aqueous alteration of GEMS-like amorphous silicate in a chondritic micrometeorite by Antarctic water. *Geochimica et Cosmochimica Acta* 293:399–421.

Tagle R. and Berlin J. 2008. A database of chondrite analyses including platinum group elements, Ni Co, Au, and Cr: Implications for the identification of chondritic projectiles. *Meteoritics & Planetary Science* 43:541–559.

Taylor S. and Brownlee D. E. 1991. Cosmic spherules in the geologic record. *Meteoritics* 26:203–211.

Taylor S., Lever J. H., and Harvey R. P. 1998. Accretion rate of cosmic spherules measured at the South Pole. *Nature* 392:899–903.

Taylor S., Lever J. H., and Harvey R. P. 2000. Numbers, types, and compositions of an unbiased collection of cosmic spherules. *Meteoritics & Planetary Science* 35:651–666.

Taylor, S., Matrajt, G., and Guan, Y. 2012. Fine-grained precursors dominate the micrometeorite flux. *Meteoritics & Planetary Science* 47:550–564.

Taylor S., Matrajt G., Lever J. H., Joswiak D. J., and Brownlee D. E. 2007. Size distribution of Antarctic micrometeorites. *Dust in Planetary Systems* 643:145–148.

Taylor S., Jones K. W., Herzog G. F., and Hornig C. E. 2011. Tomography: A window on the role of sulfur in the structure of micrometeorites. *Meteoritics & Planetary Science* 46:1498–1509.

Toppani A. and Libourel G. 2003. Factors controlling compositions of cosmic spinels: Application to atmospheric entry conditions of meteoritic materials. *Geochimica et Cosmochimica Acta* 67:4621–4638.

Toppani A., Libourel G., Engrand C., and Maurette M. 2001. Experimental simulation of atmospheric entry of micrometeorites. *Meteoritics & Planetary Science* 36:1377–1396.

Van Ginneken M., Folco L., Cordier C., and Rochette P. 2012. Chondritic micrometeorites from the Transantarctic Mountains. *Meteoritics & Planetary Science* 47:228–247.

Van Ginneken M., Genge M. J., Folco L., and Harvey R. P. 2016. The weathering of micrometeorites from the Transantarctic Mountains. *Geochimica et Cosmochimica Acta* 179:1–31.

Van Ginneken M., Gattacceca J., Rochette P., Sonzogni C., Alexandre A., Vidal V., and Genge M. J. 2017. The parent body controls on cosmic spherule texture: Evidence from the oxygen isotopic compositions of large micrometeorites. *Geochimica et Cosmochimica Acta* 212:196–210.

Yada T., Nakamura T., Takaoka N., Noguchi T., Terada K., Yano H., Nakazawa T., and Kojima H. 2004. The global accretion rate of extraterrestrial materials in the last glacial period estimated from the abundance of micrometeorites in Antarctic glacier ice. *Earth, Planets and Space* 56:67–79.

Yada T., Nakamura T., Noguchi T., Matsumoto N., Kusakabe M., Hiyagon H., Ushikubo T., Sugiura N., Kojima H., and Takaoka N. 2005. Oxygen isotopic and chemical compositions of cosmic spherules collected from the Antarctic ice sheet: Implications for their precursor materials. *Geochimica et Cosmochimica Acta* 69:5789–5804.

Yiou F., Raisbeck G. M., and Jéhanno C. 1989. Influx of cosmic spherules to the Earth during the last ~105 years as deduced from concentrations in Antarctic ice cores. *Meteoritics* 24:344.